



**HAL**  
open science

## **A novel N-substituted valine derivative with unique PPAR $\gamma$ binding properties and biological activities**

Franck Peiretti, Roberta Montanari, Davide Capelli, Bernadette Bonardo, Cécilia Colson, Ez Zoubir Amri, Marina Grimaldi, Patrick Balaguer, Giorgio Pochetti, Jean Michel Brunel

### ► To cite this version:

Franck Peiretti, Roberta Montanari, Davide Capelli, Bernadette Bonardo, Cécilia Colson, et al.. A novel N-substituted valine derivative with unique PPAR $\gamma$  binding properties and biological activities. *Journal of Medicinal Chemistry*, 2020, 63 (21), pp.13124-13139. 10.1021/acs.jmedchem.0c01555 . hal-03085059

**HAL Id: hal-03085059**

**<https://hal.science/hal-03085059>**

Submitted on 8 Jan 2021

**HAL** is a multi-disciplinary open access archive for the deposit and dissemination of scientific research documents, whether they are published or not. The documents may come from teaching and research institutions in France or abroad, or from public or private research centers.

L'archive ouverte pluridisciplinaire **HAL**, est destinée au dépôt et à la diffusion de documents scientifiques de niveau recherche, publiés ou non, émanant des établissements d'enseignement et de recherche français ou étrangers, des laboratoires publics ou privés.

## **A novel N-substituted valine derivative with unique PPAR $\gamma$ binding properties and biological activities**

Franck Peiretti,<sup>1,†,\*</sup> Roberta Montanari,<sup>2,†</sup> Davide Capelli,<sup>2</sup> Bernadette Bonardo,<sup>1</sup> Cécilia Colson,<sup>3</sup> Ez-Zoubir Amri,<sup>3</sup> Marina Grimaldi,<sup>4</sup> Patrick Balaguer,<sup>4</sup> Giorgio Pochetti,<sup>2,#</sup> and Jean Michel Brunel<sup>5,#</sup>

<sup>1</sup>Aix Marseille Univ, INSERM, INRAE, C2VN, Marseille, France

<sup>2</sup>Istituto di Cristallografia, Consiglio Nazionale delle Ricerche, Via Salaria km. 29.300, 00015, Monterotondo Stazione, Rome, Italy

<sup>3</sup>Université Côte d'Azur, CNRS, Inserm, iBV, Nice, France

<sup>4</sup>Institut de Recherche en Cancérologie de Montpellier (IRCM), Inserm, Univ Montpellier, ICM, Montpellier, France

<sup>5</sup>Aix Marseille Univ, INSERM, SSA, MCT, Marseille, France

## ABSTRACT

A proprietary library of novel N-aryl substituted amino acid derivatives bearing hydroxamate head group allowed the identification of compound **3a** that possesses weak proadipogenic and PPAR $\gamma$  activating properties. The systematic optimization of **3a**, in order to improve its PPAR $\gamma$  agonist activity, led to the synthesis of compound **7j** (N-aryl substituted valine derivative) that possesses dual PPAR $\gamma$  / PPAR $\alpha$  agonistic activity. Structural and kinetic analyses reveal that **7j** occupies the typical ligand binding domain of the PPAR $\gamma$  agonists with, however, a unique high-affinity binding mode. Furthermore, **7j** is highly effective in preventing CDK5-mediated phosphorylation of PPAR $\gamma$  serine 273. Although less proadipogenic than rosiglitazone, **7j** significantly increases adipocyte insulin-stimulated glucose uptake and efficiently promotes white-to-brown adipocyte conversion. In addition, **7j** prevents the palmitate-induced lipid accumulation in hepatoma cells. The unique biochemical properties and biological activities of compound **7j** suggest its potential efficacy in reducing insulin resistance, obesity and non-alcoholic fatty liver disease.

## INTRODUCTION

Peroxisome proliferator-activated receptors (PPAR) are transcription factors belonging to the nuclear receptor superfamily and activated by ligands such as dietary fatty acids, particularly polyunsaturated fatty acids. The three PPAR subtypes: PPAR $\alpha$ ,  $\gamma$ , and  $\delta$  ( $\beta$ ), have different, yet overlapping, tissue expression patterns <sup>1</sup> and exert major roles in the regulation of specific physiological functions including glucose and lipid metabolism and energy homeostasis <sup>2-4</sup>. These features make PPARs important molecular targets for the development of drugs for metabolic diseases.

PPAR $\alpha$  is expressed in all metabolic tissues, but predominantly in the liver where it is involved in the regulation of the uptake and oxidation of fatty acids and lipoprotein metabolism <sup>5</sup>. The fibrates family of drugs (clofibrate and fenofibrate) are pharmacological weak agonists of PPAR $\alpha$  that are used to treat dyslipidemia as they lower plasma triglycerides and increase HDL cholesterol levels <sup>6</sup>. The PPAR $\alpha$  agonist fenofibrate has also beneficial effect in patient with non-alcoholic fatty liver disease (NAFLD) characterized by the accumulation of triglycerides in hepatocytes <sup>7</sup>. However, fibrates increase markers of cardiovascular and renal disease and that of liver dysfunction, which underlines their ability to trigger adverse effects <sup>8</sup>. Therefore, efforts are being made to develop PPAR $\alpha$  agonists with improved clinical efficacy, Penafibrate being one of these new generation agonists <sup>9</sup>.

PPAR $\delta$  is involved in the regulation of fatty acid oxidation and mitochondrial respiration predominantly in skeletal muscle, liver and adipose tissue <sup>10</sup>. Therefore, agonists targeting PPAR $\delta$  may be considered as potential therapeutic agents for insulin-resistant related conditions. PPAR $\delta$  agonists have been developed and used in research <sup>11</sup> but none are currently approved for clinical use.

PPAR $\gamma$  is considered the master regulator of adipogenesis via its promotion of lipid production and storage. Thiazolidinediones, including rosiglitazone (Rosi) and pioglitazone, are the most effective PPAR $\gamma$  activating drugs that were widely prescribed for the treatment of type 2 diabetes<sup>12</sup>. However, their strong agonist activities are partly responsible for unwanted harmful side effects such as weight gain, fluid retention, osteoporosis, heart failure and cancer<sup>13,14</sup>, which precipitated their withdrawal from the market.

The quest for antidiabetic compounds targeting PPAR with good therapeutic potential and reduced adverse effects has followed two main directions. The one based on the observation that a moderate, rather than full, activation of PPAR $\gamma$  dissociates the deleterious from the therapeutic effects of the agonist has led to the generation of selective PPAR $\gamma$  modulators (SPPAR $\gamma$ M) with higher therapeutic profiles than full agonists<sup>15,16</sup>. The peculiar properties of SPPAR $\gamma$ M being explained by the ability of PPAR $\gamma$  to adopt ligand-specific conformations with different transcriptional signatures. In addition, it has been shown that the clinical benefit of PPAR $\gamma$  partial agonists and SPPAR $\gamma$ M also involves their ability to inhibit the cyclin-dependent kinase 5 (CDK5)-mediated PPAR $\gamma$  phosphorylation at serine 273<sup>17,18</sup>. The other concept for developing safe antidiabetic drugs targeting PPAR considers that beneficial effects of their activation could counteract their harmful effects. PPAR $\alpha/\gamma$  dual agonists, so-called Glitazars, that combine the insulin sensitizing effect of PPAR $\gamma$  agonists with the beneficial effect of PPAR $\alpha$  agonists on the lipid profile are representative of this class of drugs<sup>19,20</sup>. Saroglitazar is approved in India for the treatment of peculiar type of diabetic dyslipidemia and hypertriglyceridemia<sup>21,22</sup>. Moreover, dual  $\alpha/\delta$  and  $\gamma/\delta$  PPAR agonists as well as "pan" agonists acting on all three isoforms are the subject of intense investigations<sup>23-25</sup> that could lead to the generation of molecules with potential additional therapeutic indications.

This work reports a mild two-step synthesis of a library of new N-aryl substituted amino acid derivatives from commercially easily available and inexpensive reagents. The effect of these compounds, in particular the influence of substitutions on their phenyl group, was evaluated on PPARs activity and led to the development of a new balanced and potent dual PPAR $\alpha/\gamma$  agonist with unique ligand binding properties and singular biological activities that qualify it as a potential therapeutic candidate to reduce insulin resistance, obesity and NAFLD.

## RESULTS AND DISCUSSION

New N-aryl substituted amino acid derivatives bearing hydroxamate head group (head), initially designed to identify MMP inhibitors, were screened on their ability to induce spontaneous (in the absence of any other inductor) adipocyte differentiation of 3T3-L1 cells by measuring intracellular lipid accumulation. The molecule named **3a** (4-Hexyloxy-N-((S)-1-hydroxycarbonyl-2-methyl-propyl)-benzamide), that contains a L-Valine (core) and a 6 carbon atoms chain (capping group) (Figure 1A and Supplemental Figure S1A and S1B), was identified as a weak activator of adipocyte differentiation as compared with Rosi (Supplemental Figure S2). We hypothesized that **3a** increased adipocyte differentiation by activating the master regulator of adipogenesis: PPAR $\gamma$ . The PPAR $\gamma$  agonistic activity of **3a** was confirmed by the use of a luminescence-based cell-based PPAR $\gamma$  transactivation assay, in which wild-type PPAR $\gamma$  ligand binding domain (PPAR $\gamma$ -LBD) is fused to the GAL4 DNA-binding domain (PPAR $\gamma$ -LBD-GAL4) and the Firefly luciferase reporter gene is under the control of GAL4 binding elements (Figure 1A). We initiated a process to identify the domains of this molecule involved in PPAR $\gamma$  activation that would ideally lead to an optimization of its PPAR $\gamma$  agonist activity.

**Effect of the amino acid core.** Analogues of the **3a** hit were designed and synthesized through a reaction involving a two steps synthesis procedure in dichloromethane from amino acid methyl ester hydrochloride **1a-1h**, easily prepared from amino acids. By using BOP reagent as an efficient and versatile reagent for the coupling of alkyloxybenzoic acid with **1a-1h**, the synthesis of various substituted amino acid ester derivatives **2a-2h** in high chemical yields of up to 90% was achieved. It is noteworthy that the transient ester species are successfully transformed into their corresponding hydroxamic acid parent derivatives **3a-3h** by using hydroxylamine (40% H<sub>2</sub>O) in MeOH at reflux for 24 hours in yields varying from 36 to

72% (Figure 1A). Changing the L-Valine core by any other amino acid, decreased the PPAR $\gamma$  activation potency of the molecule (Figure 1A) perhaps due to a steric hindrance more important generated by the isopropyl moiety with respect to a benzyl or a hydroxy methyl group, for example.

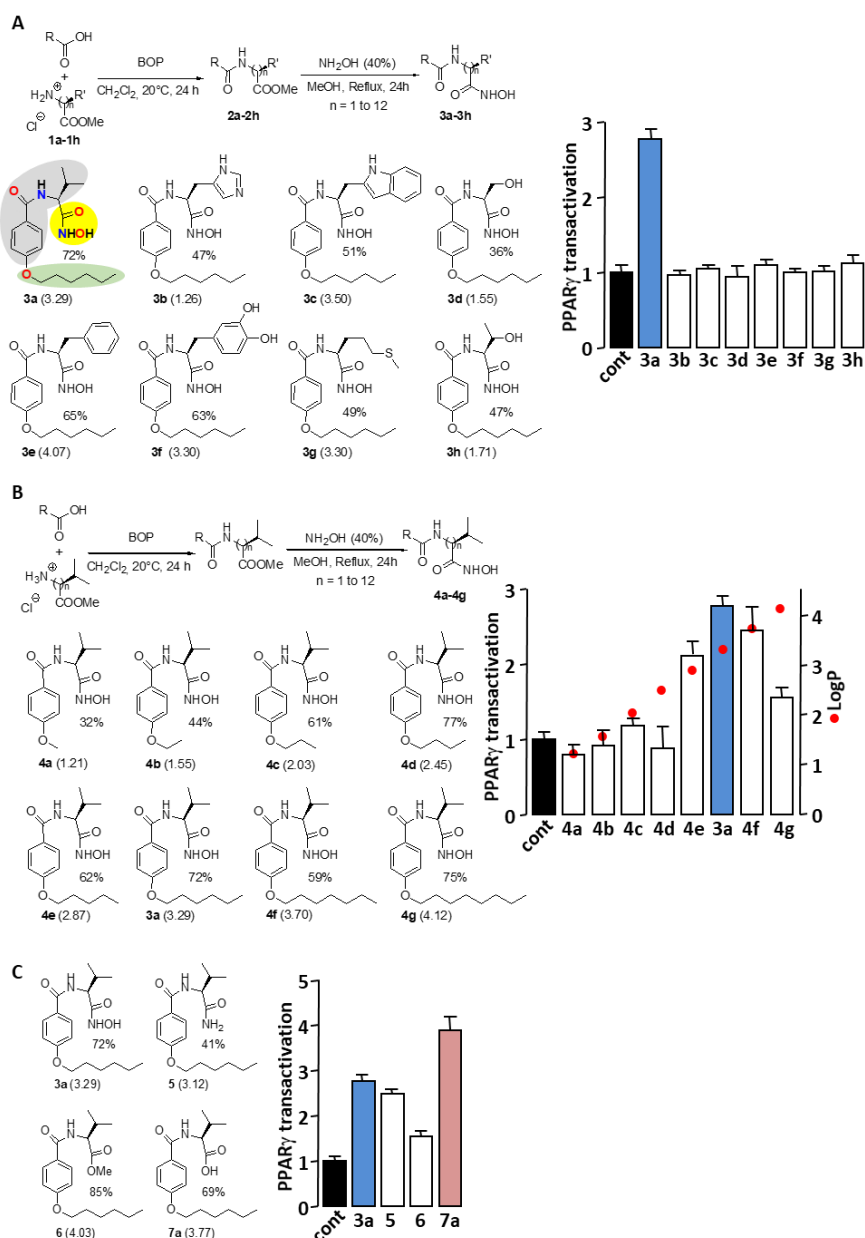


**Figure 1.** Chemical structures and PPAR $\gamma$  agonist activity of **3a** and its derivatives. The amino acid core (A), hydrophobic capping group (B) and binding head group (C) of **3a** were modified (left panels) and PPAR $\gamma$  transactivation activity of each molecule (5  $\mu$ M) was measured (right panels). Color fills accentuates the amino acid core (gray), hydrophobic capping group (green) and binding head group (yellow) of **3a**. LogP of each molecule is shown in brackets below the chemical structure and is represented by a red dot in B. The percentage indicates the yield of

the synthesis. PPAR $\gamma$  transactivation values are means  $\pm$  s.d (n = 3) expressed relative to the mean of control values, which was set to 1.

**Effect of the carbon atoms chain capping group.** The different derivatives **4a-4h** were synthesized according a similar procedure than for compounds **3a-3h** in good-to-excellent yields, varying from 32 to 75% (Figure 1B). Altering the number of carbons in the polycarbon chain capping group of the aryl moiety showed that a linear 6 carbons chain was optimal for PPAR $\gamma$  activation (Figure 1B). This result suggests that the steric hindrance and/or the hydrophobic nature of the polycarbon chain are important factors to consider when designing most potent analogues. A correlation was observed between the LogP parameter of the molecules, which reflects the true behavior and bioavailability of an ionizable compound in a solution at a physiological pH, and their ability to transactivate PPAR $\gamma$  (Figure 1B). Indeed, derivatives displaying a LogP superior to 2.5 (i.e., the most hydrophobic derivatives **3a**, **4e - 4g**) also displayed higher PPAR $\gamma$  activation whereas low activities were encountered for compounds **4a - 4d** presenting low LogP values varying from 1.21 to 2.45. However, it is unlikely that the increase in PPAR $\gamma$  transactivation related to the extension of the polycarbon chain results solely from the increased LogP of the molecules. Indeed, beyond 6 carbons atoms LogP continued to increase while the transactivation activity decreased.

**Effect of the head group.** Substitution of the hydroxamate head moiety in **3a** (Figure 1C) revealed that the preferred functions for PPAR $\gamma$  activation are OH > NHOH  $\geq$  NH<sub>2</sub> > COOMe (Figure 1C). The analog of **3a**, with a carboxylic acid moiety in place of hydroxamate head group that optimally activated PPAR $\gamma$  was named **7a**.

**Optimization of PPAR $\gamma$  agonist activity of 7a.** Changing the absolute conformation of the core Valine from L to D abolished the PPAR $\gamma$  activation capacity of **7a** (Figure 2A). Furthermore, substitution of the amino acid core (L-Valine) by other amino acid (L-form) and/or reducing

the length of the polycarbon chain decreased the PPAR $\gamma$  activation efficiency of **7a** (Figure 2B). The PPAR $\gamma$  transactivation activity of **7a** was gradually enhanced by the extension of the polycarbon chain up to 8 carbon atoms (Figure 2C). The analog of **7a** with the 8 carbon atoms chain in place of the 6 carbon atoms chain which optimally activates PPAR $\gamma$  was named **7j** (Supplemental Figure S1C and S1D). Of note, the presence of a chain with 10 carbon atoms in the molecule **7k** did not further enhance its ability to activate PPAR $\gamma$  while the LogP value is increased.

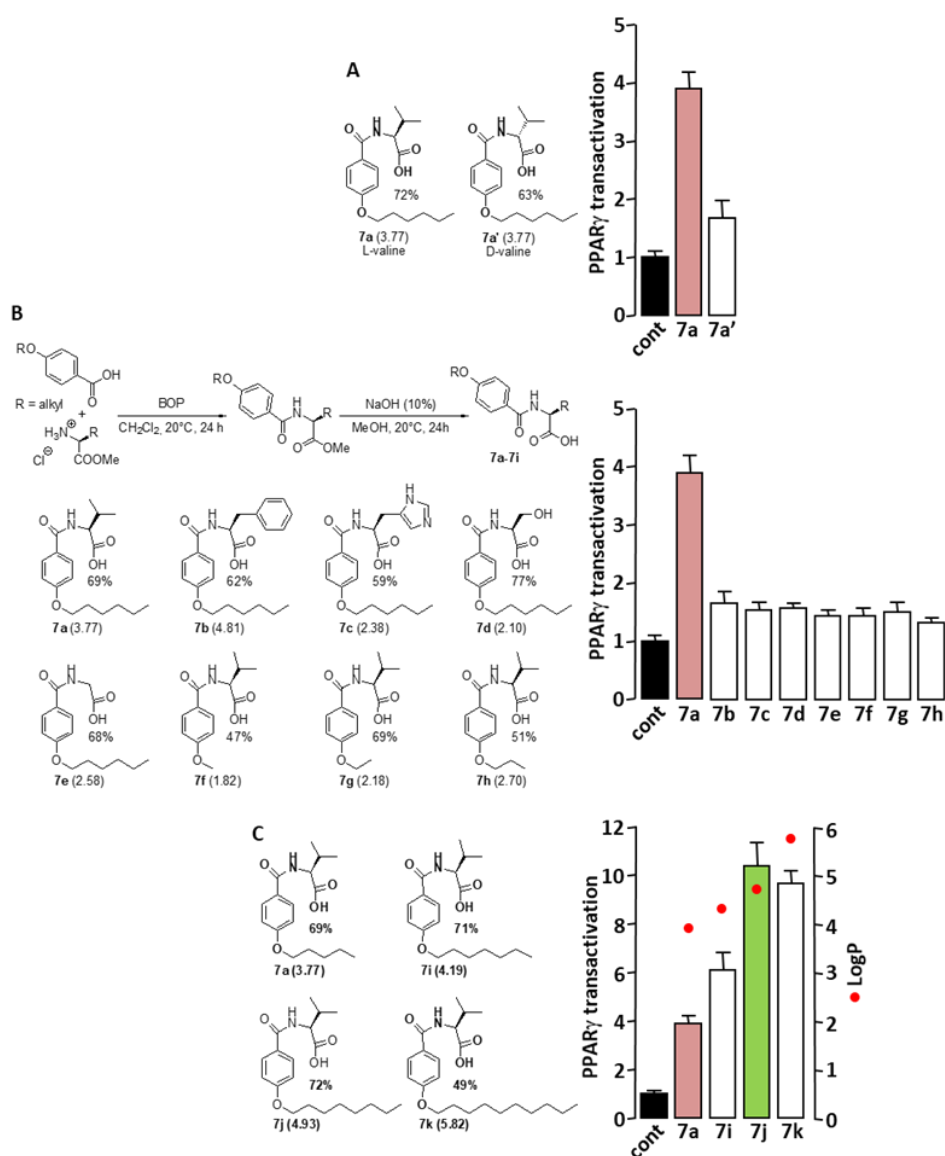


**Figure 2.** Chemical structures and PPAR $\gamma$  agonist activity of **7a** and its derivatives. The absolute conformation of the valine core (A), the amino acid core (B) or the hydrophobic capping group (B and C) of **7a** were modified (left panels) and PPAR $\gamma$

transactivation activity of each molecule (5  $\mu\text{M}$ ) was measured (right panels). LogP is shown in brackets below the chemical structure and represented by a red dot in C. The percentage indicates the yield of the synthesis. PPAR $\gamma$  transactivations are expressed as in figure 1.

Typical PPAR agonists are known to consist of three parts: a polar head group (usually bearing a carboxylic acid functionality), a hydrophobic tail moiety and a linker which consists of flexible methylene units and an aromatic ring <sup>26</sup>. Interestingly, **7a** and **7j** closely meet these elementary criteria.

**Potency and efficacy of PPAR $\gamma$  activation.** The dose-dependent activation of PPAR $\gamma$  by the "hit" compound **3a** and its two "lead" derivatives **7a** and **7j** were compared to that of the PPAR $\gamma$  full agonist Rosi using *PPAR $\gamma$ -LBD-GAL4* chimera assay (Figure 3A).

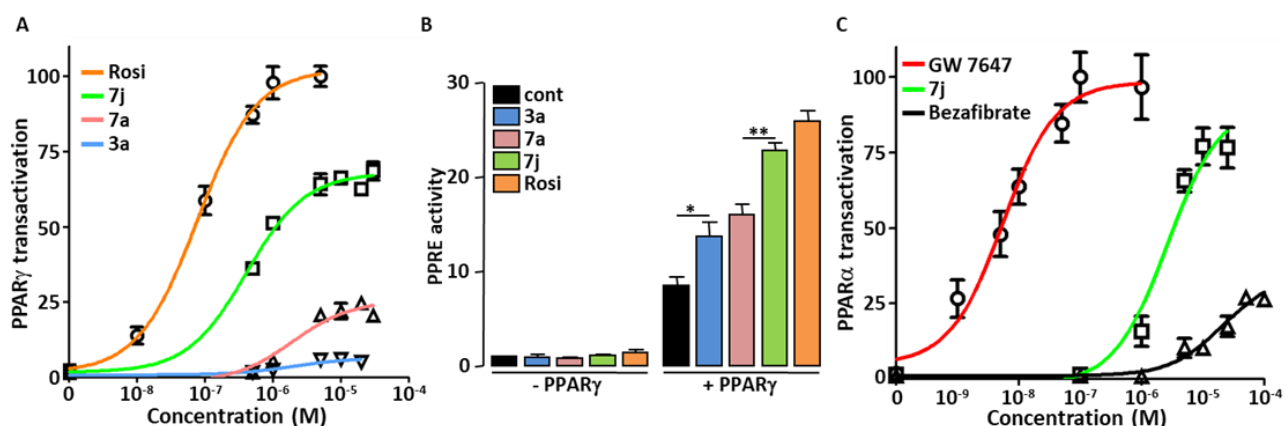


**Figure 3.** PPAR agonist activity of **3a**, **7a** and **7j**. (A) Concentration-dependent PPAR $\gamma$  transactivation activities of **3a**, **7a** and **7j** were compared to that of Rosi using *PPAR $\gamma$ -LBD-GAL4* chimera assay. Values are expressed as % of the maximal response measured with Rosi (5  $\mu\text{M}$ ). (B) HEK293 cells were transfected with PPRE-driven Firefly luciferase and SV40-driven Renilla luciferase coding vectors together with an empty plasmid (-PPAR $\gamma$ ) or with the PPAR $\gamma$  expression vector (+PPAR $\gamma$ ). 36 hours post transfection, cells were incubated for 17 hours with **3a**, **7a**, **7j** (1 $\mu\text{M}$ ) or Rosi (0.1 $\mu\text{M}$ ). PPRE promoter activity was calculated as the ratio Firefly/Renilla luciferase. Values are means  $\pm$  s.d (n = 5) expressed relative to the control situation. \*p < 0.05, \*\*p < 0.01 (one-way ANOVA followed by Bonferroni's *post hoc* test). (C) Concentration-dependent PPAR $\alpha$  transactivation activities of **7j**, GW 7647 and Bezafibrate were measured using *PPAR $\alpha$ -LBD-GAL4* chimera assay. Values are expressed as % of the maximal response measured with GW 7647 (1  $\mu\text{M}$ ).

The potencies of the compounds were ranked as follow: **3a**  $\approx$  **7a** < **7j** < Rosi (Table 1). Regarding their efficacy (maximal PPAR $\gamma$  transactivation) compounds were ranked as follow: **3a** < **7a** < **7j**  $\leq$  Rosi (Table 1).

Compound	PPAR	EC <sub>50</sub> (nM)	Activity (%)
Rosi	$\gamma$	76 $\pm$ 30	100
<b>7j</b>	$\gamma$	400 $\pm$ 150	66.36 $\pm$ 3.41
<b>7a</b>	$\gamma$	1940 $\pm$ 940	25.06 $\pm$ 2.03
<b>3a</b>	$\gamma$	1840 $\pm$ 1020	6.33 $\pm$ 1.03
GW 7647	$\alpha$	5.4 $\pm$ 1	100
<b>7j</b>	$\alpha$	2910 $\pm$ 920	98.2 $\pm$ 5.53
Bezafibrate	$\alpha$	31700 $\pm$ 5410	35.4 $\pm$ 3.81

**Table 1.** EC<sub>50</sub> and maximal activation of PPAR $\gamma$  and PPAR $\alpha$

Activities are expressed as % of the maximal response measured with 5  $\mu$ M of Rosi (for PPAR $\gamma$ ) or with 1  $\mu$ M of GW 7647 (for PPAR $\alpha$ ). Values are means  $\pm$  s.d (n = 3).

PPAR $\gamma$  activation elicited by **7j** was around 70% of that obtained with Rosi. However, **7j** reduced the Renilla luciferase expression (Supplemental Figure S3A), used to normalize the values of the reporter gene for variations inherent to transfection efficiency and sample handling, making difficult to assess its true levels of PPAR $\gamma$  activation. Indeed, taking account of Renilla luciferase expression values to calculate PPAR $\gamma$  activation dose-response curves significantly increased the maximal response triggered by **7j** (Supplemental Figure S3B). This side effect of **7j** is not strictly related to a toxic effect as the reduction in Renilla luciferase expression occurred at lower concentrations than those causing reduction of cellular ATP content (Supplemental Figure S3C). Moreover, Rosi that poorly reduced Renilla luciferase expression was not less toxic than **7j** (Supplemental Figure S3C). Taken together, these data

allow us to define **3a** and **7a** as partial agonists of PPAR $\gamma$  and **7j** as a strong partial agonist of PPAR $\gamma$ .

A PPAR Responsive Element (PPRE)-based luciferase assay was carried out to assess the ability of **3a**, **7a** and **7j** to transactivate genes controlled by the binding of PPAR $\gamma$  to PPRE. The three molecules increased the expression of PPRE-driven luciferase only when full-length PPAR $\gamma$  was expressed (Figure 3B), showing that these molecules stimulate the actual transcriptional activity of PPAR $\gamma$ . Interestingly, the transactivation efficiencies were in agreement with those measured by the PPAR $\gamma$ -LBD-GAL4 chimera assay, i.e. **3a**  $\leq$  **7a** < **7j**  $\leq$  Rosi.

Some compounds with moderate PPAR $\gamma$  agonist activity (partial agonists or modulators) maintain significant anti-diabetic activity while having fewer and/or less severe adverse effects than full PPAR $\gamma$  agonists<sup>27</sup>. Therefore, **3a**, **7a** and **7j** can reasonably be considered as scaffold molecules to develop new anti-diabetic drugs.

**Specificity.** The dose-dependent activations of PPAR $\delta$  and PPAR $\alpha$  by **3a**, **7a** and **7j** were analyzed using the appropriate PPAR-LBD-GAL4 chimera assays. None of the molecules activated PPAR $\delta$  (Supplemental Figure S4). Only **7j** transactivated PPAR $\alpha$  (Figure 3C and Table 1), with potency between that of Bezafibrate (a weak pan agonist for all three PPAR isoforms) and GW 7647 (a full PPAR $\alpha$  agonist). **7j** appeared to be a full PPAR $\alpha$  agonist.

Therefore, **7j** is a dual PPAR $\gamma/\alpha$  agonist (Glitazar) and as such, it could theoretically have beneficial synergistic activities on glucose and lipid homeostasis<sup>19,20</sup>.

**Binding of 7j to PPAR $\gamma$ .** The crystal structure of the complex of PPAR $\gamma$  LBD with the ligand **7j** was solved collecting diffraction data from apo-crystals soaked for three days in the presence of the ligand at 0.5 mM. Initial difference Fourier maps revealed clear electron density for the ligand (Supplemental Figure S5) showing that it occupies the typical LBD region of the PPAR $\gamma$  agonists (Figure 4A), similar to that of the full agonist Rosi (Figure 4B), with its

carboxylate group directly interacting through H-bonds with Y473 of helix 12 (H12), at the short distance of 2.3 Å, the two histidines (H323 and H449) of the canonical triad, and S289, (Figure 4A). The NH of **7j** amide bond is also involved in a H-bond with S289 and the CO makes a H-bond with Y327. The terminal aliphatic chain of **7j** is in equilibrium between two different conformations (occupation factors of 0.6 and 0.4, respectively) and makes vdW contacts with several residues of the internal strand of the  $\beta$ -sheet, as shown in Figure 4A, with a consequent effective stabilization of this domain. The isopropyl terminal group of **7j**, makes vdW interactions in the hydrophobic pocket formed by the residues F282, C285, Q286, L453 and L469 (belonging to H3, H11 and H12), contributing in this way to a tighter binding of the ligand (Figure 4C).

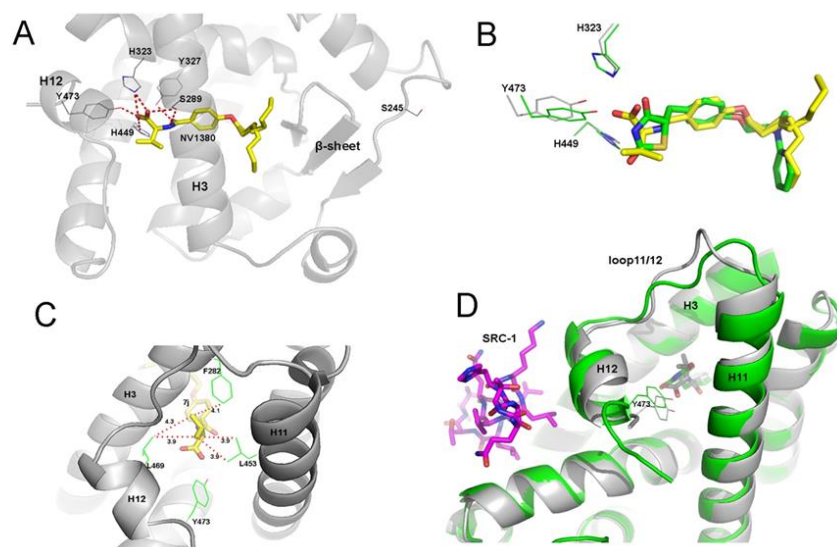


**Figure 4.** Binding of **7j** to PPAR $\gamma$ . (A) Hydrogen-bond network of **7j** in the PPAR $\gamma$  LBD. (B) Superimposition of **7j** (yellow) and Rosi (green) structures. (C) vdW network of the **7j** with residues belonging to H3, H11 and H12 of the PPAR $\gamma$  LBD. (D) Superimposition of **7j** (yellow) and Rosi (green) with the co-activator SRC-1 (magenta); the PPAR $\gamma$  / Rosi structure is colored in green, PPAR $\gamma$  / **7j** in gray.

The thorough analysis of the effective binding network of **7j** into the PPAR $\gamma$  LBD indicates that the ligand is very tightly locked into the LBD, with its carboxylate group strongly

interacting with Y473 of H12 (2.3 Å), but in a slightly distorted mode, with respect to Rosi. As a consequence, there is an adjustment of the conformation of H12, the loop 11/12 and the beginning of H11 (Figure 4D), with respect to Rosi, that could affect the binding of co-activator, possibly determining the partial agonism of **7j**.

Interestingly, a similar unique binding network was observed in the PPAR $\gamma$  crystal structure with the partial agonist SR2067 (Supplemental Figure S6)<sup>28</sup>. Both ligands share a common amide group that forms two hydrogen bonds with Y327 and S289, interactions that are not possible with Rosi. However, unlike **7j**, SR2067 does not interact with Y473.

It is commonly accepted that a PPAR $\gamma$  partial agonist is likely to have anti-diabetic provided that it combines low transactivation activity with high binding affinity<sup>29</sup>. Therefore, the affinity ( $K_d$ ) and rate constants ( $k_{on}$ ,  $k_{off}$ ) of PPAR $\gamma$  for the partial agonist **7j** were compared with those of PPAR $\gamma$  for the reference ligand Rosi using surface plasmon resonance (Table 2 and Supplemental Figure S7).

Interaction	$k_{on}$ ( $M^{-1}s^{-1}$ )	$k_{off}$ ( $s^{-1}$ )	$K_d$ (nM)
PPAR $\gamma$ /Rosi	4.1 (0.4) $10^5$	0.102 (0.005)	250 (30)
PPAR $\gamma$ / <b>7j</b>	2.9 (0.2) $10^5$	0.044 (0.001)	150 (10)

**Table 2.** Affinity ( $K_d$ ) and rate constants ( $k_{on}$ ,  $k_{off}$ ) for PPAR $\gamma$ /ligand interactions. Experimental error is reported in brackets.

Remarkably, **7j** shows an affinity towards PPAR $\gamma$  similar or higher than Rosi. These results confirm that the partial agonism of **7j** can be the result of a unique high-affinity binding which, although similar to that of the full agonist Rosi, slightly alters the active conformation of AF2 surface, a necessary requirement for recruiting co-activators.

Moreover, it is known that partial agonists of PPAR $\gamma$  preferentially stabilize the  $\beta$ -sheet region of the LBD. In the PPAR $\gamma$ /**7j** structure, the long aliphatic chain of the ligand strongly contributes

to the stabilization of this region, through vdW interactions, with both its observed conformations facing residues of the innermost  $\beta$ -strand. The solvent entropic gain arising from a more efficacious displacement of water molecules, known to occupy the  $\beta$ -sheet pocket, could play an important role in lowering the free energy of the binding.

**CDK5-mediated phosphorylation of PPAR $\gamma$ .** Part of the anti-diabetic effects of PPAR $\gamma$  partial agonists have been associated with their ability to prevent the CDK5-mediated phosphorylation of PPAR $\gamma$  serine 273 residue<sup>17,18</sup>. Therefore, we assessed the ability of **7j** to inhibit such a phosphorylation. An ELISA protocol was optimized to quantify the phosphorylation of PPAR $\gamma$  triggered *in vitro* by recombinant CDK5. **7j** prevented the phosphorylation of PPAR $\gamma$  serine 273 at least as efficiently as Rosi (Figure 5A).

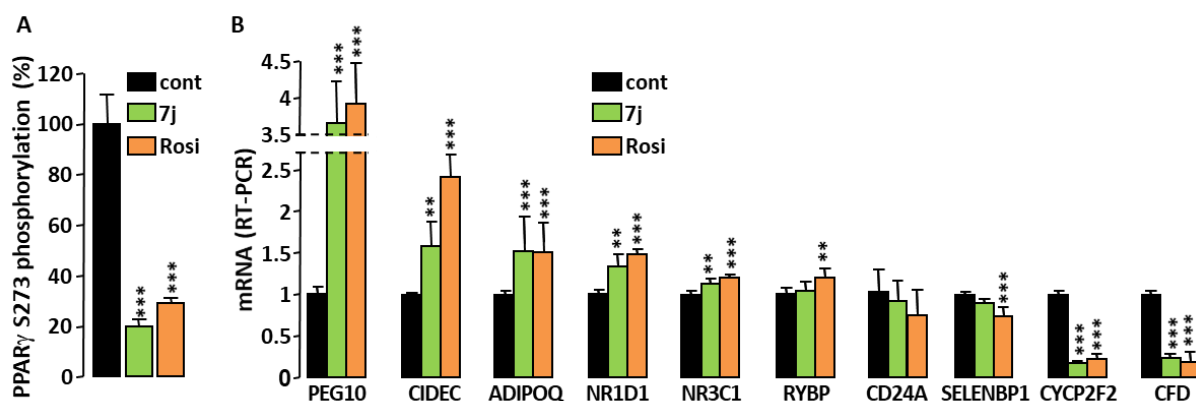


**Figure 5.** Effect of **7j** on PPAR $\gamma$  phosphorylation. (A) Percentage of *in vitro* PPAR $\gamma$  Ser273 phosphorylation by CDK5 in the presence of 0.1  $\mu$ M of **7j** or Rosi. (B) RT-PCR analysis of the expression levels of a selection of genes known to be regulated by CDK5-dependent phosphorylation of PPAR $\gamma$ . Values are means  $\pm$  s.d (n = 5) expressed relative to the mean of control. \*\*p < 0.01, \*\*\*p < 0.001 vs. control (one-way ANOVA followed by Dunnett's *post hoc* test)

The ability of **7j** to prevent CDK5-mediated phosphorylation of PPAR $\gamma$  was also studied in 3T3-L1 adipocytes. Out of ten genes known to be significantly controlled by CDK5-dependent PPAR $\gamma$  phosphorylation in fully differentiated adipocytes<sup>17,18</sup>, seven were regulated in the same way by **7j** and Rosi (Figure 5B). Two genes were only regulated by Rosi and the expression of one gene was not significantly modified by **7j** and Rosi, although both molecules

tended to alter this expression in the same direction. These results underline the ability of **7j** to reduce CDK5-mediated phosphorylation of PPAR $\gamma$  serine 273 and to alter the expression of genes controlled by PPAR $\gamma$  phosphorylation. This feature supports a potential anti-diabetic effect of **7j**.

**Adipocyte differentiation and glucose uptake.** Adipogenesis-mediated weight gain is a major side effect of PPAR $\gamma$  full agonists<sup>30</sup>. Partial PPAR $\gamma$  agonists are expected to have a reduced effect on lipid storage while maintaining a significant insulin sensitization effect. Therefore, the proadipogenic properties of **3a**, **7a** and **7j** were compared to that of Rosi. 3T3-L1 fibroblast cells were incubated in the presence of PPAR $\gamma$  agonists as the sole inducer of adipocyte differentiation. Only **7j** and Rosi (the strongest PPAR $\gamma$  agonists) significantly increased the intracellular lipid content (Figure 6A and Supplemental Figure S8), showing that these two molecules stimulate adipocyte differentiation. However, for the same concentration, the proadipogenic property of **7j** was significantly lower than that of Rosi. When 3T3-L1 fibroblast cells were primed for adipocyte differentiation using the conventional adipogenic cocktail (Insulin, Dexamethasone, IBMX) and then treated for 7 days with the **3a**, **7a**, **7j** or Rosi, mRNA levels of the markers of adipocyte differentiation were all increased in proportion to the ability of the molecules to activate PPAR $\gamma$  (Figure 6B). As expected for partial PPAR $\gamma$  agonists, **3a**, **7a** and **7j** have reduced proadipogenic properties compared with the full agonist Rosi.

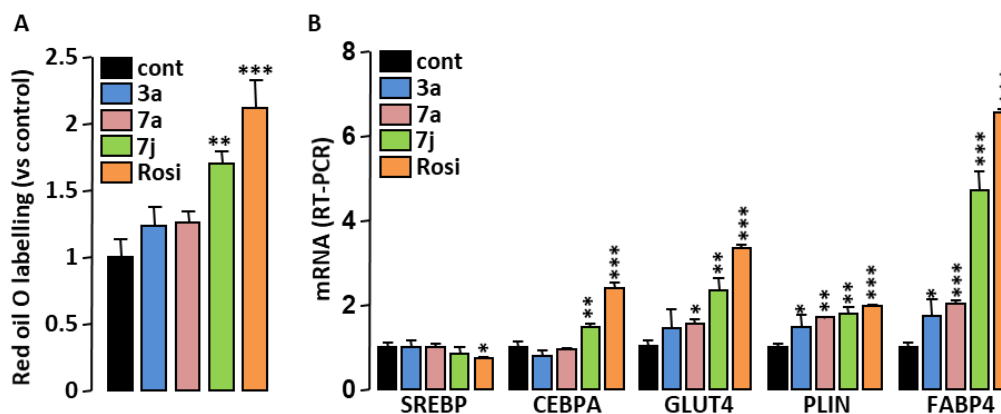


**Figure 6.** Adipogenic effect of the compounds. (A) 3T3-L1 fibroblasts were incubated for 6 days with insulin (350 nM) and the indicated PPAR $\gamma$  agonists (1  $\mu$ M). Intracellular lipids were stained with Red Oil O then colored lipids were quantified. (B) 3T3-L1 adipocyte differentiation was triggered by the standard mixture of inducers then cells were incubated for 7 days with **3a**, **7a**, **7j** (1  $\mu$ M) or Rosi (0.1  $\mu$ M). The expression levels of adipogenesis-related genes were measured by RT-PCR. Values are means  $\pm$  s.d. (n = 5) expressed as fold relative to untreated situation. \*p < 0.05, \*\*p < 0.01, \*\*\*p < 0.001 vs. control (one-way ANOVA followed by Dunnett's *post hoc* test).

It has been shown that the ability of PPAR $\gamma$  ligands to increase cellular glucose uptake is not necessarily related to their transactivation activity or proadipogenic potential<sup>31</sup>. Therefore, glucose uptake was measured in fully differentiated 3T3-L1 adipocytes after an acute treatment with PPAR $\gamma$  agonists. The insulin-dependent glucose uptake was increased by a short-term treatment with **7j** or Rosi (Figure 7), denoting that part of their insulin sensitizing effect is independent of their ability to increase adipocyte differentiation.

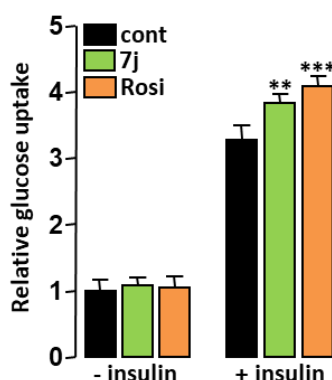


**Figure 7.** Adipocyte glucose uptake. 3T3-L1 adipocytes were treated with **7j** (1  $\mu$ M) or Rosi (0.1  $\mu$ M) for 16 h prior insulin stimulation (50 nM; 10 min) and cellular glucose uptake was determined. Values are mean  $\pm$  s.d. (n = 4) expressed as fold relative to the control situation. \*\*p < 0.01, \*\*\*p < 0.001 vs. control (one-way ANOVA followed by Dunnett's *post hoc* test).

**Adipocyte browning.** Brown fat is a target for anti-obesity and anti-diabetes experimental therapies that aim to increase energy expenditure <sup>32</sup>. Interestingly, strong PPAR $\gamma$  agonists activate the “browning” of white adipose tissues <sup>33,34</sup>, suggesting that partial PPAR $\gamma$  agonists that retain significant white fat browning ability may also have therapeutic benefits in the treatment of obesity and diabetes. We therefore studied the ability of **3a**, **7a** and **7j** to induce brite/brown-like adipocytes in 3T3-L1 cells. Only **7j** increased mRNA levels of genes considered as brite/brown adipocyte markers (Figure 8A, B) <sup>35</sup>. Coherent with their adipocyte browning effect, Rosi and **7j** increased mRNA levels of additional genes involved in (or associated with) mitochondria biogenesis (Figure 8C) <sup>36</sup> and in accordance these two molecules significantly increased the selective labeling of active mitochondria by the MitoTracker dye (Figure 8D). We have previously shown that Rosi induced the conversion of hMADS white adipocytes into brite adipocytes as evidenced by the strong expression of UCP1 <sup>37</sup>. In order to test whether compounds **3a**, **7a** and **7j** were able to substitute for Rosi, hMADS cells first differentiated into white adipocytes were treated with these compounds between days 14 and 18. UCP1 mRNA expression was analyzed as an indicator of the degree of white-to-brown adipocyte conversion. UCP1 mRNA levels were increased in **3a**, **7a** and **7j** -treated cells compared to untreated cells and **7j** was found to be the most potent compound (Figure 8E). Moreover, UCP1 mRNA levels were similarly increased by 300 nM of **7j** or 100 nM of Rosi (Figure 8F). The expression of the adipogenic marker Perilipin was not modified by Rosi or **7j** (Supplemental Figure S9A), whereas the expression of Adiponectin, a PPAR $\gamma$ -responsive gene, was more efficiently increased by Rosi than by **7j** (Supplemental Figure S9B), which confirms the that the PPAR $\gamma$  agonist activity of **7j** is lower than that of Rosi.

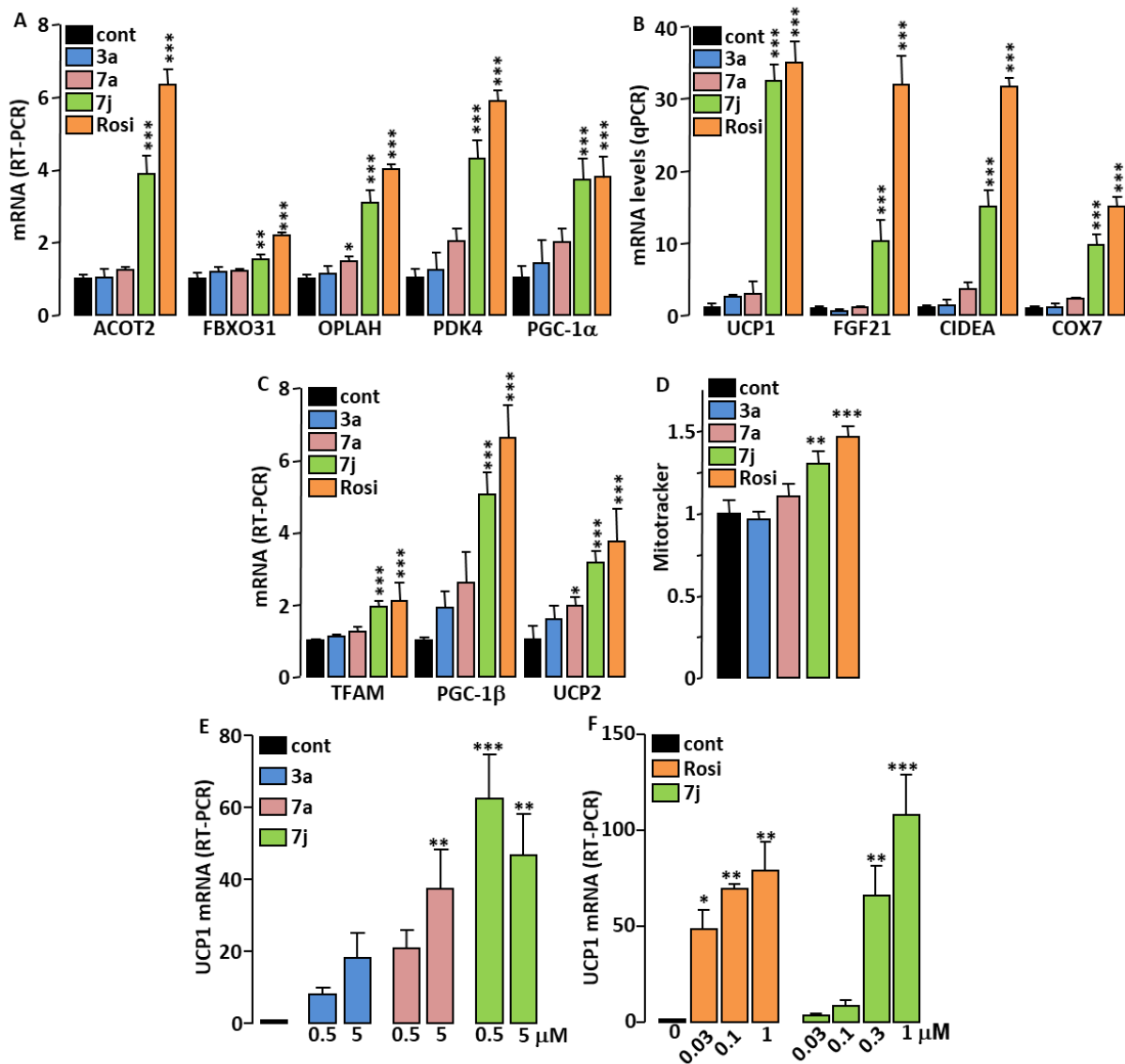


**Figure 8.** Adipocyte browning effect of the compounds. 3T3-L1 were treated as in Figure 6B then expression levels of beige (A) and brown (B) adipocyte markers as well as those of genes involved in mitochondrial biogenesis (C) were measured by RT-PCR. (D) Adipocyte mitochondria content was evaluated by flow cytometry after their selective labeling with MitoTracker dye. (E, F) hMADS white adipocytes were treated with the indicated compounds and UCP1 mRNA levels were measured by RT-PCR. Values are mean  $\pm$  s.d. (n = 5) expressed as fold relative to the control (cont) situation. \*p < 0.05, \*\*p < 0.01, \*\*\*p < 0.001 vs. control (one-way ANOVA followed by Dunnett's *post hoc* test).

These data show that **7j** represents a potential and novel therapy targeting adipose tissue based on its potency to activate PPAR pathways, in order to combat obesity and associated diseases *via* the recruitment and activation of thermogenic adipocytes.

**Hepatocytes lipid accumulation.** As PPAR $\alpha$  agonists decrease hepatic steatosis<sup>5,7</sup>, we compared the effect of **7j** (a dual PPAR $\alpha/\gamma$  agonist) to that of Rosi (PPAR $\gamma$  agonist) on the lipid accumulation into HuH7 hepatoma cells. Both compounds impeded the basal intracellular lipid accumulation, however only **7j** efficiently prevented the palmitate-induced lipid accumulation (Figure 9), suggesting **7j** as a promising compound in the treatment of NAFLD.

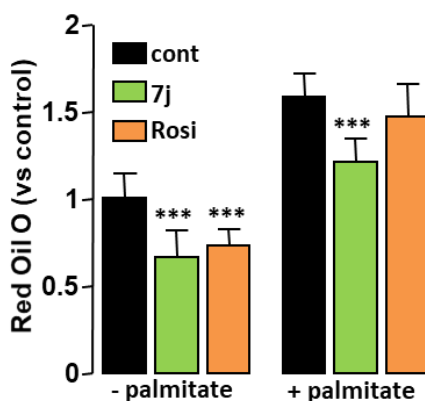


**Figure 9.** Hepatocyte lipid uptake. Confluent HuH7 hepatoma cells were treated with **7j** or Rosi (0.5  $\mu$ M) for 24 hours prior the addition of palmitate (1 mM). 24 hours later, cellular lipid content was measured using Red Oil O staining. Values are mean  $\pm$  s.d. (n = 5) expressed as fold relative to the control (cont). \*\*\*p < 0.001 vs. control (one-way ANOVA followed by Dunnett's *post hoc* test).

## CONCLUSION

We have described the synthesis and optimization of compound **7j**: a new N-aryl substituted valine derivative with a balanced agonist activity on PPAR  $\alpha$  and  $\gamma$ . Compound **7j** occupies the typical LBD region of the PPAR $\gamma$  agonists with a unique high-affinity binding mode and efficiently prevents CDK5-mediated phosphorylation of PPAR $\gamma$ . While poorly proadipogenic, compound **7j** increases adipocyte insulin-stimulated glucose uptake and efficiently promotes white-to-brown adipocyte conversion. In addition, compound **7j** impedes the palmitate-induced lipid accumulation in hepatoma cells. The unique biochemical properties and *in vitro* biological activities of compound **7j** suggest its potential effectiveness in reducing insulin resistance, obesity and NAFLD.

## EXPERIMENTAL SECTION

### 1. Chemistry

All solvents were purified according to reported procedures, and reagents were used as commercially available. Methanol, ethyl acetate, dichloromethane, ammonia and petroleum ether (35-60°C) were purchased from VWR and used without further purification. Column chromatography was performed on VWR silica gel (70-230 mesh).  $^1\text{H}$  NMR and  $^{13}\text{C}$  NMR spectra were recorded in  $\text{CDCl}_3$  or  $\text{DMSO-d}_6$  on a Bruker AC 300 spectrometer working at 300 MHz and 75 MHz, respectively (the usual abbreviations are used: s: singlet, d: doublet, t: triplet, q: quadruplet, m: multiplet). Tetramethylsilane was used as internal standard. All chemical shifts are given in ppm. Purity of all the new compounds is up to 99% and has been evaluated by HPLC analysis (Agilent 1100, C18).

#### **Typical procedure for the synthesis of amino acids methyl ester hydrochloride derivatives**

##### Synthesis of L-Valine methyl ester hydrochloride

In a two necked round flask equipped with a condenser were placed at room temperature 3 g of L-Valine ( $2.56 \cdot 10^{-2}$  mol) in 20 mL of methanol. The mixture was placed under stirring at 0°C and 3.4 mL of thionylchloride ( $4.7 \cdot 10^{-3}$  mol) were slowly added. After removal of the solvents, diethylether was added and the product precipitate as a white solid. After filtration the product was dried under vacuum to afford the expected L-Valine methyl ester hydrochloride in 86% yield.

White solid;  $^1\text{H}$  NMR ( $\text{D}_2\text{O}$ ):  $\delta = 4.14\text{-}4.17$  (m, 1H),  $3.80\text{-}3.85$  (m, 3H),  $2.50\text{-}2.56$  (m, 1H),  $1.12\text{-}1.15$  (m, 6H).  $^{13}\text{C}$  ( $\text{D}_2\text{O}$ ):  $\delta = 168.91, 58.57, 53.02, 29.95, 18.15$ .

### Synthesis of (*S*)-2-(4-Hexyloxy-benzoylamino)-3-methyl-butyrac acid methyl ester **6**

In a two necked round flask equipped with a condenser were placed at room temperature 2.34 g of benzotriazol-1-yloxytris(dimethylamino)phosphonium hexafluorophosphate (BOP;  $5.26 \cdot 10^{-3}$  mol), 2.34 mL of diisopropylethylamine ( $1.8 \cdot 10^{-2}$  mol), 1.2 g of 4-(Hexyloxy)benzoic acid ( $5.40 \cdot 10^{-3}$  mol) and 0.88 g of L-Valine methyl ester hydrochloride ( $5.25 \cdot 10^{-3}$  mol) in 15 mL of  $\text{CH}_2\text{Cl}_2$ . The mixture was placed under stirring at room temperature for 24 hours. Water was added to allow phase separation. The bottom phase layer was washed with  $\text{NaHCO}_3$  (10%) solution, dried over  $\text{Na}_2\text{SO}_4$ , filtered and concentrated in vacuo. After removal of the solvents, the crude residue was purified by chromatography on a silicagel column using  $\text{CH}_2\text{Cl}_2$ /Ethylacetate (1/1) eluent affording the expected product **6** in 85% yield.

White solid;  $^1\text{H}$  NMR ( $\text{CDCl}_3$ ):  $\delta$  = 8.06 (m, 2H), 7.15 (m, 2H), 4.15-4.22 (m, 4H), 3.71-3.75 (m, 3H), 1.81-2.05 (m, 3H), 1.21-1.37 (m, 6H), 0.69-0.92 (m, 9H).  $^{13}\text{C}$  ( $\text{CDCl}_3$ ):  $\delta$  = 172.90, 166.54, 160.52, 133.08, 130.21, 130.01, 114.55, 68.22, 57.56, 52.34, 33.49, 31.32, 29.34, 25.67, 22.61, 18.48, 14.03. MS (ESI)  $\text{C}_{19}\text{H}_{29}\text{NO}_4$   $m/z$  336.2146 (100%, ( $\text{M}+\text{H}^+$ )).

### Synthesis of 4-Hexyloxy-N-((*S*)-1-hydroxycarbamoyl-2-methyl-propyl)-benzamide **3a**

In a 25 mL round flask were placed at room temperature 0.6 g of **6** ( $1.78 \cdot 10^{-3}$  mol) in 15 mL of ethanol. 2 mL of a hydroxylamine solution (40%) were subsequently added and the mixture was allowed to stir at reflux for 24 hours. After removal of the solvents, the crude residue was purified by chromatography on a silicagel column using petroleum ether/ethylacetate (1/1) then methanol/ethylacetate (1/1) as eluents affording the expected product **3a** in 72% yield.

White solid;  $^1\text{H}$  NMR ( $\text{DMSO } d_6$ ):  $\delta$  = 8.01 (m, 2H), 7.09 (m, 2H), 3.95-3.98 (m, 3H), 1.78-1.82 (m, 2H), 1.01-1.31 (m, 6H), 0.71-0.93 (m, 9H).  $^{13}\text{C}$  ( $\text{DMSO } d_6$ ):  $\delta$  = 167.20, 166.23, 161.1, 133.41,

129.80, 113.98, 69.41, 57.31, 31.03, 29.42, 25.76, 22.43, 18.62, 13.89. MS (ESI)  $C_{18}H_{28}N_2O_4$   $m/z$  337.2045 (100%, (M+H<sup>+</sup>)).

4-Hexyloxy-N-[(S)-1-hydroxycarbamoyl-2-(3H-imidazol-4-yl)-ethyl]-benzamide **3b**

Procedure similar to that applied for the preparation of **3a**

Pale yellow solid; <sup>1</sup>H NMR (DMSO d6):  $\delta$  = 7.52-7.89 (m, 3H), 6.89-7.42 (m, 5H), 5.55 (s, 2H), 4.75-4.73 (m, 2H), 4.10-4.19 (m, 2H), 1.22-1.92 (m, 9H), 0.89-0.96 (m, 3H). <sup>13</sup>C (DMSO d6):  $\delta$  = 174.19, 164.07, 162.03, 133.17, 129.03, 123.47, 118.22, 115.35, 67.56, 52.96, 30.99, 30.91, 29.05, 25.49, 22.54, 14.25. MS (ESI)  $C_{19}H_{26}N_4O_4$   $m/z$  375.2014 (100%, (M+H<sup>+</sup>)).

4-Hexyloxy-N-[(S)-1-hydroxycarbamoyl-2-(1H-indol-2-yl)-ethyl]-benzamide **3c**

Procedure similar to that applied for the preparation of **3a**

White solid; <sup>1</sup>H NMR (DMSO d6):  $\delta$  = 7.32-7.62 (m, 5H), 6.29-7.25 (m, 7H), 3.92-4.03 (m, 2H), 2.89-3.34 (m, 4H), 1.20-1.79 (m, 6H), 0.88-0.92 (m, 3H). <sup>13</sup>C (DMSO d6):  $\delta$  = 172.22, 168.98, 161.25, 139.48, 131.05, 129.14, 126.29, 120.15, 118.78, 113.69, 110.36, 104.25, 71.24, 53.32, 30.21, 28.28, 25.14, 22.04, 14.13. MS (ESI)  $C_{24}H_{29}N_3O_4$   $m/z$  424.2236 (100%, (M+H<sup>+</sup>)).

4-Hexyloxy-N-((S)-2-hydroxy-1-hydroxycarbamoyl-ethyl)-benzamide **3d**

Procedure similar to that applied for the preparation of **3a**

White solid; <sup>1</sup>H NMR (DMSO d6):  $\delta$  = 7.02-7.51 (m, 4H), 3.62-4.20 (m, 5H), 1.31-1.82 (m, 9H), 0.89-0.92 (m, 3H). <sup>13</sup>C (DMSO d6):  $\delta$  = 170.36, 168.24, 160.89, 130.14, 125.34, 113.47, 68.78, 61.24, 53.89, 31.01, 28.14, 25.98, 21.33, 13.88. MS (ESI)  $C_{16}H_{24}N_2O_5$   $m/z$  325.1768 (100%, (M+H<sup>+</sup>)).

4-Hexyloxy-N-((S)-1-hydroxycarbamoyl-2-phenyl-ethyl)-benzamide **3e**

Procedure similar to that applied for the preparation of **3a**

White solid;  $^1\text{H}$  NMR (DMSO  $d_6$ ):  $\delta$  = 7.66-7.68 (m, 2H), 6.47-7.16 (m, 2H), 3.55-3.97 (m, 2H), 2.89-3.23 (m, 2H), 1.35-1.74 (m, 8H), 0.90-0.91 (m, 3H).  $^{13}\text{C}$  (DMSO  $d_6$ ):  $\delta$  = 178.45, 168.32, 161.25, 137.47, 129.02, 125.68, 114.98, 60.01, 53.87, 40.36, 30.23, 28.14, 24.12, 22.98, 13.48. MS (ESI)  $\text{C}_{22}\text{H}_{28}\text{N}_2\text{O}_4$   $m/z$  385.2057 (100%, ( $\text{M}+\text{H}^+$ )).

N-[(S)-2-(3,4-Dihydroxy-phenyl)-1-hydroxycarbamoyl-ethyl]-4-hexyloxy-benzamide **3f**

Procedure similar to that applied for the preparation of **3a**

White solid;  $^1\text{H}$  NMR (DMSO  $d_6$ ):  $\delta$  = 7.71-7.73 (m, 2H), 6.59-6.93 (m, 4H), 6.32 (s, 1H), 5.87 (s, 1H), 3.99-4.02 (m, 2H), 2.95-2.99 (m, 2H), 1.17-2.02 (m, 9H), 0.87-0.89 (m, 3H).  $^{13}\text{C}$  (DMSO  $d_6$ ):  $\delta$  = 171.25, 168.33, 160.58, 146.01, 143.69, 128.69, 126.47, 123.74, 116.36, 115.47, 69.71, 52.34, 38.38, 28.47, 22.14, 25.69, 22.47, 13.12. MS (ESI)  $\text{C}_{22}\text{H}_{28}\text{N}_2\text{O}_6$   $m/z$  417.1934 (100%, ( $\text{M}+\text{H}^+$ )).

4-Hexyloxy-N-((S)-1-hydroxycarbamoyl-4-methylsulfanyl-butyl)-benzamide **3g**

Procedure similar to that applied for the preparation of **3a**

White solid;  $^1\text{H}$  NMR (DMSO  $d_6$ ):  $\delta$  = 6.91-7.69 (m, 5H), 1.17-2.74 (m, 20H), 0.87-0.88 (m, 3H).  $^{13}\text{C}$  (DMSO  $d_6$ ):  $\delta$  = 170.78, 168.65, 162.21, 128.12, 125.14, 117.77, 69.66, 51.45, 34.12, 31.78, 28.02, 25.63, 22.33, 15.15, 13.19. MS (ESI)  $\text{C}_{19}\text{H}_{30}\text{N}_2\text{O}_4\text{S}$   $m/z$  383.1935 (100%, ( $\text{M}+\text{H}^+$ )).

4-(hexyloxy)-N-((2S,3S)-3-hydroxy-1-(hydroxyamino)-1-oxobutan-2-yl)benzamide **3h**

Procedure similar to that applied for the preparation of **3a**

White solid;  $^1\text{H}$  NMR (DMSO  $d_6$ ):  $\delta$  = 7.71-7.73 (m, 2H), 6.98-7.11 (m, 3H), 5.32 (s, 1H), 4.60-4.65 (m, 1H), 4.06-4.44 (m, 3H), 1.80-1.92 (m, 1H), 1.07-1.37 (m, 12H);  $^{13}\text{C}$  (DMSO  $d_6$ ):  $\delta$  = 169.75, 167.63, 162.54, 132.53, 125.82, 114.51, 68.78, 67.63, 59.34, 31.88, 28.02, 24.89, 22.33, 15.12, 13.89. MS (ESI)  $\text{C}_{17}\text{H}_{26}\text{N}_2\text{O}_5$   $m/z$  339.1879 (100%, (M+H $^+$ )).

(S)-N-(1-(hydroxyamino)-3-methyl-1-oxobutan-2-yl)-4-methoxybenzamide **4a**

White solid;  $^1\text{H}$  NMR (DMSO  $d_6$ ):  $\delta$  = 0.91-0.96 (m, 6H), 2.16-2.23 (m, 1H), 3.84 (s, 3H), 4.33-4.45 (m, 1H), 6.98-7.53 (m, 2H), 7.83-7.89 (m, 2H), 8.79 (s, 2H);  $^{13}\text{C}$  (DMSO  $d_6$ ):  $\delta$  = 174.44, 170.42, 164.51, 130.95, 127.71, 115.17, 56.40, 52.96, 32.19, 20.12, 19.65. MS (ESI)  $\text{C}_{13}\text{H}_{18}\text{N}_2\text{O}_4$   $m/z$  267.1386 (100%, (M+H $^+$ )).

(S)-4-ethoxy-N-(1-(hydroxyamino)-3-methyl-1-oxobutan-2-yl)benzamide **4b**

White solid;  $^1\text{H}$  NMR (DMSO  $d_6$ ):  $\delta$  = 0.91-0.95 (m, 6H), 1.49 (t,  $J$  = 7.0 Hz, 3H), 1.68-1.75 (m, 1H), 4.01-4.11 (m, 2H), 4.31-4.41 (m, 1H), 6.94-6.99 (m, 2H), 7.80-7.85 (m, 2H), 8.59 (s, 2H);  $^{13}\text{C}$  (DMSO  $d_6$ ):  $\delta$  = 171.10, 166.47, 166.91, 132.01, 129.30, 114.59, 63.42, 56.95, 30.10, 18.64, 14.69. MS (ESI)  $\text{C}_{14}\text{H}_{20}\text{N}_2\text{O}_4$   $m/z$  281.1412 (100%, (M+H $^+$ )).

(S)-N-(1-(hydroxyamino)-3-methyl-1-oxobutan-2-yl)-4-propoxybenzamide **4c**

White solid;  $^1\text{H}$  NMR (DMSO  $d_6$ ):  $\delta$  = 0.92-1.12 (m, 9H), 1.69-1.89 (m, 2H), 3.27-3.38 (m, 2H), 3.90-4.02 (m, 2H), 6.90-7.07 (m, 2H), 7.76-7.89 (m, 2H);  $^{13}\text{C}$  (DMSO  $d_6$ ):  $\delta$  = 171.14, 165.95, 162.22, 130.95, 128.03, 115.09, 70.35, 57.03, 30.75, 22.63, 18.64, 10.63. MS (ESI)  $\text{C}_{15}\text{H}_{22}\text{N}_2\text{O}_4$   $m/z$  294.1634 (100%, (M+H $^+$ )).

(S)-4-butoxy-N-(1-(hydroxyamino)-3-methyl-1-oxobutan-2-yl)benzamide **4d**

White solid;  $^1\text{H}$  NMR (DMSO  $d_6$ ):  $\delta$  = 0.90-0.98 (m, 9H), 1.52-1.62 (m, 2H), 1.77-1.83 (m, 2H), 2.16-2.22 (m, 2H), 3.97-4.02 (m, 2H), 4.37-4.42 (m, 1H), 7.75-7.77 (m, 2H), 7.98-8.02 (m, 2H), 8.53 (m, 1H);  $^{13}\text{C}$  (DMSO  $d_6$ ):  $\delta$  = 171.49, 166.14, 166.16, 133.37, 130.18, 122.86, 69.16, 57.04, 30.74, 30.69, 18.48, 13.75. MS (ESI)  $\text{C}_{16}\text{H}_{24}\text{N}_2\text{O}_4$   $m/z$  309.1701 (100%,  $(\text{M}+\text{H}^+)$ ).

(S)-N-(1-(hydroxyamino)-3-methyl-1-oxobutan-2-yl)-4-(pentyloxy)benzamide **4e**

White solid;  $^1\text{H}$  NMR (DMSO  $d_6$ ):  $\delta$  = 0.90-0.98 (m, 9H), 1.52-1.62 (m, 2H), 1.77-1.83 (m, 2H), 2.16-2.22 (m, 2H), 3.97-4.02 (m, 2H), 4.37-4.42 (m, 1H), 7.75-7.77 (m, 2H), 7.98-8.02 (m, 2H), 8.53 (m, 1H);  $^{13}\text{C}$  (DMSO  $d_6$ ):  $\delta$  = 169.71, 167.51, 162.83, 132.86, 126.86, 119.98, 68.72, 58.13, 31.14, 30.98, 29.34, 28.14, 18.54, 14.16. MS (ESI)  $\text{C}_{17}\text{H}_{26}\text{N}_2\text{O}_4$   $m/z$  323.1934 (100%,  $(\text{M}+\text{H}^+)$ ).

(S)-4-(heptyloxy)-N-(1-(hydroxyamino)-3-methyl-1-oxobutan-2-yl)benzamide **4f**

White solid;  $^1\text{H}$  NMR (DMSO  $d_6$ ):  $\delta$  = 0.90-0.96 (m, 9H), 1.28-1.74 (m, 10H), 2.02-2.16 (m, 1H), 3.97-4.07 (m, 2H), 4.37-4.42 (m, 1H), 7.03-7.08 (m, 2H), 8.02-8.09 (m, 2H), 8.53 (m, 1H);  $^{13}\text{C}$  (DMSO  $d_6$ ):  $\delta$  = 171.09, 166.42, 162.02, 130.07, 129.03, 115.18, 68.15, 57.63, 31.80, 29.18, 26.04, 22.14, 18.74, 13.98. MS (ESI)  $\text{C}_{19}\text{H}_{30}\text{N}_2\text{O}_4$   $m/z$  351.2245 (100%,  $(\text{M}+\text{H}^+)$ ).

(S)-N-(1-(hydroxyamino)-3-methyl-1-oxobutan-2-yl)-4-(octyloxy)benzamide **4g**

White solid;  $^1\text{H}$  NMR (DMSO  $d_6$ ):  $\delta$  = 0.90-0.97 (m, 9H), 1.29-1.82 (m, 12H), 2.06-2.15 (m, 1H), 3.95-4.07 (m, 2H), 4.32-4.41 (m, 1H), 7.00-7.08 (m, 2H), 8.01-8.10 (m, 2H), 8.51 (m, 1H);  $^{13}\text{C}$  (DMSO  $d_6$ ):  $\delta$  = 171.10, 166.35, 162.35, 131.37, 129.90, 115.11, 68.24, 57.52, 31.79, 30.95, 29.31, 26.82, 22.47, 18.63, 14.21. MS (ESI)  $\text{C}_{20}\text{H}_{32}\text{N}_2\text{O}_4$   $m/z$  365.2423 (100%,  $(\text{M}+\text{H}^+)$ ).

Synthesis of (*S*)-2-(4-Hexyloxy-benzoylamino)-3-methyl-butyric acid **7a**.

In a 25 mL round flask were placed at room temperature 0.6 g of **6** ( $1.78 \cdot 10^{-3}$  mol) in 15 mL of ethanol. 2 mL of a sodium hydroxide solution (10%) were subsequently added and the mixture was allowed to stir at room temperature for 24 hours. The bottom phase layer was discarded, and the aqueous phase was acidified with HCl 1N. After extraction with ethylacetate, the organic phase was dried over Na<sub>2</sub>SO<sub>4</sub>, filtered and concentrated in vacuo. The crude residue was purified by chromatography on a silicagel column using petroleum ether/ethylacetate (1/1) as eluent affording the expected product **7a** in 69% yield.

White solid; <sup>1</sup>H NMR (CDCl<sub>3</sub>): δ = 6.54-7.14 (m, 4H), 3.89-3.98 (m, 3H), 1.51-2.14 (m, 7H), 0.89-1.34 (m, 11H). <sup>13</sup>C (CDCl<sub>3</sub>): δ = 177.57, 166.34, 159.95, 132.32, 130.12, 114.07, 72.30, 64.36, 31.32, 31.03, 29.14, 25.32, 22.14, 18.48, 13.95. MS (ESI) C<sub>18</sub>H<sub>27</sub>NO<sub>4</sub> m/z 322.1932 (100%, (M+H<sup>+</sup>)).

(*R*)-2-(4-Hexyloxy-benzoylamino)-3-methyl-butyric acid **7a'**

Procedure similar to that applied for the preparation of **7a**

White solid; <sup>1</sup>H NMR (CDCl<sub>3</sub>): δ = 6.55-7.19 (m, 4H), 3.89-3.99 (m, 3H), 1.50-2.11 (m, 7H), 0.89-1.32 (m, 11H). <sup>13</sup>C (CDCl<sub>3</sub>): δ = 177.56, 166.34, 159.95, 132.36, 130.12, 114.08, 72.30, 64.36, 31.32, 31.04, 29.14, 25.31, 22.14, 18.47, 13.96. MS (ESI) C<sub>18</sub>H<sub>27</sub>NO<sub>4</sub> m/z 322.1932 (100%, (M+H<sup>+</sup>)).

(*S*)-2-(4-Hexyloxy-benzoylamino)-3-phenyl-propionic acid **7b**

Procedure similar to that applied for the preparation of **7a**

White solid; <sup>1</sup>H NMR (CDCl<sub>3</sub>): δ = 10.98 (s, 1H), 7.89-8.01 (m, 2H), 6.95-7.21 (m, 7H), 4.83-4.85 (m, 11H), 3.89-3.92 (m, 2H), 3.01-3.03 (m, 2H), 0.95-1.61 (m, 12H). <sup>13</sup>C (CDCl<sub>3</sub>): δ = 176.15,

168.13, 161.14, 140.03, 129.18, 128.82, 123.52, 123.42, 115.22, 73.34, 61.56, 38.78, 33.14, 31.42, 26.14. MS (ESI) C<sub>23</sub>H<sub>30</sub>NO<sub>4</sub> m/z 385.2221 (100%, (M+H<sup>+</sup>)).

(S)-2-(4-Hexyloxy-benzoylamino)-3-(3H-imidazol-4-yl)-propionic acid **7c**

Procedure similar to that applied for the preparation of **7a**

Yellow solid; <sup>1</sup>H NMR (CDCl<sub>3</sub>): δ = 7.93 (s, 1H), 7.63-7.65 (m, 2H), 6.75-6.92 (m, 4H), 4.69-4.72 (m, 2H), 4.12-3.92 (m, 2H), 2.67-2.78 (m, 2H), 0.76-1.52 (m, 11H). <sup>13</sup>C (CDCl<sub>3</sub>): δ = 174.75, 169.70, 161.08, 132.04, 131.03, 129.92, 125.75, 121.56, 111.04, 68.13, 52.67, 31.14, 29.57, 29.15, 25.56, 22.59, 13.82. MS (ESI) C<sub>19</sub>H<sub>25</sub>N<sub>3</sub>O<sub>4</sub> m/z 360.1834 (100%, (M+H<sup>+</sup>)).

(S)-2-(4-Hexyloxy-benzoylamino)-3-hydroxy-propionic acid **7d**

Procedure similar to that applied for the preparation of **7a**

White solid; <sup>1</sup>H NMR (DMSO d<sub>6</sub>): δ = 7.68 (s, 2H), 6.92-6.96 (m, 2H), 3.92-4.54 (m, 6H), 1.20-1.95 (m, 9H), 0.89-0.92 (m, 3H). <sup>13</sup>C (DMSO d<sub>6</sub>): δ = 173.32, 166.74, 161.44, 128.45, 125.18, 111.14, 68.84, 62.30, 56.14, 31.12, 29.11, 24.13, 22.59, 14.13. MS (ESI) C<sub>16</sub>H<sub>23</sub>NO<sub>5</sub> m/z 310.1667 (100%, (M+H<sup>+</sup>)).

(4-Hexyloxy-benzoylamino)-acetic acid **7e**

Procedure similar to that applied for the preparation of **7a**

White solid; <sup>1</sup>H NMR (DMSO d<sub>6</sub>): δ = 7.68 (s, 2H), 6.98 (s, 2H), 4.10-4.12 (m, 2H), 3.78 (m, 2H), 1.49-1.76 (m, 8H), 0.89-0.92 (m, 3H). <sup>13</sup>C (DMSO d<sub>6</sub>): δ = 172.31, 168.28, 161.02, 130.06, 114.55, 114.53, 66.42, 42.85, 34.56, 32.12, 29.14, 23.12, 21.45, 14.14. MS (ESI) C<sub>15</sub>H<sub>21</sub>NO<sub>4</sub> m/z 280.1511 (100%, (M+H<sup>+</sup>)).

(S)-2-(4-Methoxy-benzoylamino)-3-methyl-butyrac acid **7f**

Procedure similar to that applied for the preparation of **7a**

White solid;  $^1\text{H}$  NMR (DMSO  $d_6$ ):  $\delta$  = 7.53-7.55 (m, 2H), 6.95-6.97 (m, 2H), 6.05 (s, 1H), 4.75-4.77 (m, 1H), 3.72 (s, 3H), 1.75-1.87 (m, 1H), 1.04-1.06 (m, 6H).  $^{13}\text{C}$  (DMSO  $d_6$ ):  $\delta$  = 172.33, 167.28, 160.14, 131.12, 127.30, 110.15, 58.66, 55.65, 30.93, 19.03. MS (ESI)  $\text{C}_{13}\text{H}_{17}\text{NO}_4$   $m/z$  251.1232 (100%, (M+H $^+$ )).

(S)-2-(4-Ethoxy-benzoylamino)-3-methyl-butyrac acid **7g**

Procedure similar to that applied for the preparation of **7a**

White solid;  $^1\text{H}$  NMR (DMSO  $d_6$ ):  $\delta$  = 7.59 (s, 2H), 7.02-7.05 (m, 2H), 4.16-4.40 (m, 3H), 1.87-1.92 (m, 1H), 1.32-1.36 (m, 3H), 0.98-1.03 (m, 6H).  $^{13}\text{C}$  (DMSO  $d_6$ ):  $\delta$  = 173.15, 167.10, 160.83, 129.98, 127.04, 113.21, 61.89, 57.93, 29.98, 19.19, 14.31. MS (ESI)  $\text{C}_{14}\text{H}_{19}\text{NO}_4$   $m/z$  266.1342 (100%, (M+H $^+$ )).

(S)-3-Methyl-2-(4-propoxy-benzoylamino)-butyrac acid **7h**

Procedure similar to that applied for the preparation of **7a**

White solid;  $^1\text{H}$  NMR (DMSO  $d_6$ ):  $\delta$  = 6.95-7.32 (m, 4H), 6.75 (s, 1H), 3.98-4.05 (m, 3H), 1.54-1.89 (m, 3H), 1.12-1.17 (m, 3H), 0.97-1.02 (m, 6H).  $^{13}\text{C}$  (DMSO  $d_6$ ):  $\delta$  = 172.34, 167.42, 160.15, 128.64, 127.42, 112.45, 69.37, 58.62, 29.89, 21.12, 18.82, 10.29. MS (ESI)  $\text{C}_{15}\text{H}_{21}\text{NO}_4$   $m/z$  280.1534 (100%, (M+H $^+$ )).

(4-(heptyloxy)benzoyl)-L-valine **7i**

White solid;  $^1\text{H}$  NMR (DMSO  $d_6$ ):  $\delta$  = 0.93-1.41 (m, 19H), 1.41-1.46 (m, 2H), 2.23-2.35 (m, 1H), 3.87-3.92 (t,  $J$  = 5Hz, 2H), 4.46-4.69 (m, 1H), 6.82-6.89 (m, 2H), 7.66-7.69 (m, 2H);  $^{13}\text{C}$  (DMSO

d6):  $\delta$  = 175.24, 167.12, 162.78, 129.02, 114.39, 68.28, 57.84, 31.80, 31.27, 29.14, 29.07, 25.98, 22.64, 19.15, 17.92, 14.12. MS (ESI)  $C_{19}H_{29}NO_4$  m/z 336.2165 (100%, (M+H<sup>+</sup>)).

**(4-(octyloxy)benzoyl)-L-valine 7j**

White solid; <sup>1</sup>H NMR (DMSO d6):  $\delta$  = 0.91-1.34 (m, 10H), 1.38-1.54 (m, 11H), 1.76-1.87 (m, 2H), 2.23-2.37 (m, 1H), 4.0.3-4.08 (t, *J* = 5Hz, 2H), 4.48-4.52 (dd, *J* = 5Hz, 1H), 6.98-7.01 (m, 2H), 7.83-8.86 (m, 2H); <sup>13</sup>C (DMSO d6):  $\delta$  = 175.31, 170.16, 163.59, 130.46, 127.28, 115.21, 69.24, 59.88, 33.04, 31.82, 30.53, 30.46, 30.34, 27.19, 23.77, 19.79, 18.97, 14.49. MS (ESI)  $C_{20}H_{31}NO_4$  m/z 350.2315 (100%, (M+H<sup>+</sup>)).

**(4-(decyloxy)benzoyl)-L-valine 7k**

White solid; <sup>1</sup>H NMR (DMSO d6):  $\delta$  = 0.92-1.32 (m, 10H), 1.44-1.54 (m, 15H), 1.82-1.88 (m, 2H), 2.33-2.46 (m, 1H), 3.94-4.06 (m, 2H), 4.82-4.87 (m, 1H), 6.86-6.94 (m, 2H), 7.73-7.83 (m, 2H) <sup>13</sup>C (DMSO d6):  $\delta$  = 175.36, 167.71, 162.20, 129.31, 129.10, 125.71, 114.33, 114.15, 68.25, 57.62, 31.94, 31.43, 29.61, 29.43, 29.37, 29.16, 26.03, 22.73, 19.09, 17.91, 14.18. MS (ESI)  $C_{22}H_{35}NO_4$  m/z 378.2645 (100%, (M+H<sup>+</sup>)).

**Cell culture.** 3T3-L1 cells (from ATCC) were routinely cultured in DMEM with 4 mM l-glutamine, 4.5 g/liter glucose, 0.11 g/liter sodium pyruvate, and supplemented with 10% fetal bovine serum plus antibiotics. Two days after confluence, adipocytes differentiation was triggered by changing the adding the conventional induction mixture (0.1  $\mu$ M dexamethazone, 500  $\mu$ M 3-Isobutyl-1-methylxanthine, and 174.5 nM insulin). After 48 h, the medium was removed and replaced by a fresh medium containing only 174.5 nM insulin. HuH7 hepatoma cells from the Japanese Cancer Research Resources Bank were cultured in DMEM containing

10% fetal bovine serum. At the confluence, cells were treated for 24 hours with 0.5 mM palmitic acid complexed with BSA. The establishment, characterization and culture protocols of human Multipotent Adipose-Derived Stem (hMADS) cells have been described previously<sup>38</sup>. Briefly, confluent cells were submitted to differentiation medium (DMEM/Ham's F12 media containing 10 µg/ml transferrin, 10 nM insulin, and 0.2 nM triiodothyronine) supplemented with 1 µM dexamethasone and 500 µM isobutyl-methylxanthine. Two days later, the medium was changed, dexamethasone and isobutyl-methylxanthine were omitted and 100 nM Rosi were added for the indicated periods. Cells were treated between days 2 and 9 with Rosi to enable white adipocyte differentiation to take place. After 5 days in the absence of Rosi, white adipocyte conversion was induced by adding compounds to be tested (day 14). Medium was changed every other day and cells were used at day 18.

**Oil Red O staining.** 3T3-L1 or HuH7 hepatoma cells were washed with PBS and fixed with 4% formaldehyde solution for 20 minutes, then washed again and stained with 0.35% Oil Red O solution in 60% isopropanol for 20 minutes. Then, cells were washed with water, and photographs were taken. The stain from the cells was eluted using 100% isopropanol and the absorbance of the eluted stain was read at 490 nm.

**2-deoxy-D-glucose uptake assay.** Glucose uptake activity of fully differentiated 3T3-L1 adipocytes was measured by the chemiluminescent assay<sup>39</sup> using Glucofax kit as described by the manufacturer (Yelen, Ensues la Redonne, France).

**Real Time PCR Analysis.** Total RNA was extracted using a Nucleospin RNA kit (Macherey-Nagel, Hoerd, France), cDNA was synthesized from 0.5 µg of RNA using Moloney murine leukemia virus reverse transcriptase (Invitrogen) and used for PCR amplification. Real Time PCR (RT-PCR) were performed on the LightCycler 480 instrument (Roche Applied Science) using the Eva Green MasterMix (Euromedex, Souffelweyersheim, France). The comparative Ct method ( $2^{-(\Delta\Delta CT)}$ ) was used to calculate the relative differences in mRNA expression. The acidic ribosomal phosphoprotein P0 (*Rplp0*) was used as housekeeping gene. Changes were normalized to the mean of control values, which was set to 1. Primer sequences were previously published <sup>17,35,38</sup>.

**MitoTracker staining.** 3T3-L1 adipocytes were trypsinized and centrifuged at 300 g at 4°C for 5 min. Cells were suspended in Kreb's Ringer solution buffered with HEPES and 0.5% BSA and incubated with 0.1 µM MitoTracker Green FM for 30 min at 37°C. Cells were spun at 300 g at 4°C for 5 min and suspended in 400 µl of fresh KRBH then analyzed using a BD Accuri C6 flow cytometer (BD Biosciences).

**Cell-based PPAR transactivation assay.** *PPAR $\gamma$ -LBD-Gal4* or *PPAR $\alpha$ -LBD-Gal4* expression vector was transfected along with SV40-driven Renilla luciferase expression vector in HEK293 cells stably expressing the Gal4 response element driven Firefly luciferase reporter. 36 hours after transfection, cells were exposed to the tested compounds for additional 16 hours then Firefly and Renilla luciferase activities were measured in the cell lysates using the reagent Genofax A and C (Yelen) in an Ensign multimode reader (Perkin Elmer). PPAR transactivation activity of the compounds is calculated as ratio of Firefly to Renilla luciferase activity.

**In vitro kinase assay.** The assay was performed on WT-PPAR $\gamma$  in the apo form and in the complex with **7j** and Rosi. For the kinase assay, stock solutions of ligands were prepared by diluting with 100% DMSO to a concentration of 50 mM. The stock solutions were further diluted with 50 mM Tris HCl pH 7.5 up to the final concentrations of 0.1  $\mu$ M, 1  $\mu$ M and 10  $\mu$ M respectively, and pre-equilibrated overnight at 4°C with the protein. Kinase assay was carried out at 30 °C for 3.5 hours in 300  $\mu$ L of buffer containing 50 mM Tris HCl pH 7.5, 7.2  $\mu$ g.mL<sup>-1</sup> PPAR $\gamma$ , 0.1-1-10  $\mu$ M ligand, 25 mM MgCl<sub>2</sub>, 50  $\mu$ M DTT, 2 mM ATP, 0.66 ng mL<sup>-1</sup> CDK5/p35 (Sigma Aldrich code n. SRP5011).

**ELISA of PPAR $\gamma$  phosphorylation.** Polystyrene micro well plates were coated overnight at 4°C with the reaction mixture, then washed three times with PBS + Tween 0.005% and left to block in PBS containing 1% bovine serum for 90 min at 37°C. The wells were washed three times and incubated for 60 min at 37°C with 100  $\mu$ L of anti-phospho-Ser/Thr-Pro antibody (Sigma Aldrich code n. A05368) diluted 1:500 in PBS. After three washes, 100  $\mu$ L of Anti-Mouse IgG-Peroxidase antibody produced in goat (Sigma Aldrich code n. A4416; 1:1000 in PBS) were added to the wells and incubated 60 min at 37°C. The wells were washed and 200  $\mu$ L of o-phenylenediamine dihydrochloride (Sigmafast OPD code n. P9187) dissolved in water were added to the wells. Optical density was measured at 450nm using ApplyScan Thermofisher Reader and the data were processed using Excel.

**Crystallization and Data Collection.** PPAR $\gamma$  LBD was expressed as N-terminal His-tagged proteins using a pET28 vector and purified as previously described<sup>40</sup>. Crystals of apo-PPAR $\gamma$  were obtained by vapor diffusion at 18°C using a sitting drop made by mixing 2  $\mu$ L of protein solution with 2  $\mu$ L of reservoir solution (0.8 M Na Citrate, 0.15M Tris, pH 8.0). The crystals

were soaked for three days in a storage solution (1.2 M Na Citrate, 0.15 M Tris, pH 8.0) containing the ligand **7j** (0.5 mM). The ligand dissolved in DMSO (50 mM) was diluted in the storage solution so that the final concentration of DMSO was 1%. The storage solution with glycerol 20% (v/v) was used as cryoprotectant. Crystals (0.15 x 0.15 mm) of PPAR $\gamma$ /**7j** belong to the space group *C2* with cell parameters shown in Table 1 of Supporting Information.

**Structure Determination and Refinement.** X-ray data set were collected at 100 K under a nitrogen stream using synchrotron radiation (beamline ID30B at ESRF, Grenoble, France). The collected data were processed using the programs Mosflm and Scala<sup>41</sup>. Structure solution was performed with AMoRe<sup>42</sup>, using the coordinates of PPAR $\gamma$ /LT175R (27) (PDB code 3D6D) as the starting model. The coordinates were then refined with CNS<sup>43</sup> and with PHENIX<sup>44</sup> including data between 58.2 and 2.0 Å. The statistics of crystallographic data and refinement are summarized in Table 1 of Supporting Information. The coordinates and structure factors for the PPAR $\gamma$ /**7j** structure described here have been deposited in the PDB under accession number 6QJ5.

**Surface Plasmon Resonance.** Surface plasmon resonance analyses were performed by using Pioneer AE optical biosensor equipped with COOH5 chips (SensiQ). PPAR $\gamma$  surfaces were prepared by using standard amine-coupling procedures<sup>45</sup> and HBS (Hepes-buffered saline: 10 mM Hepes, 150 mM NaCl, 0.005% P20, DMSO 1%, pH 7.4) as the running buffer. Flow cells were activated for 7 min by injecting 140  $\mu$ L of 50 mM *N*-hydroxysuccinimide (NHS):200 mM ethyl-3(3-dimethylamino) propylcarbodiimide (EDC). 150  $\mu$ L of a 0.25 mg/mL PPAR $\gamma$  solution (in 10 mM NaOAc, pH 5.0) were injected for 15 min at 10  $\mu$ L/min on channels 1 and 3 (channel 2 was used as reference, for a duplicate

experiment), followed by a 70  $\mu\text{L}$  injection of ethanolamine to block any remaining activated groups on the surface. 12,220 and 7500 RU of protein were immobilized on channel 1 and 3, respectively. The screening of the analytes (**7j** and Rosi) was performed using HBS, with 1% DMSO. To collect detailed kinetic data the OneStep<sup>46</sup> protocol was used, injecting the analytes at a flow rate of 50  $\mu\text{L}/\text{min}$  and at the concentration of 1  $\mu\text{M}$  over the two channels at 20  $^{\circ}\text{C}$  (association phase of 180 s). Four buffer blanks were injected for double referencing. The regeneration of the surfaces between binding cycles was not necessary because all the analytes dissociate quickly in the 120 s dissociation phase. A DMSO calibration plot was constructed (buffer sample containing 0-2% (vol/vol) DMSO) to correct for bulk refractive index shifts. All sensorgrams were processed by using double referencing. To obtain kinetic rate constants and affinity constants the corrected response data were fit in the program QDAT. A kinetic analysis of each ligand/analyte interaction was obtained by fitting the response data to a 1:1 bimolecular interaction model. The equilibrium dissociation constant ( $K_d$ ) was determined by the ratio  $k_{\text{off}}/k_{\text{on}}$ .

**Statistical Analyses.** Statistical significance was estimated with one-way ANOVA followed by Bonferroni or Dunnett *post hoc* test or with *F*-Test using Graph Pad Prism version 5.0 (GraphPad Software, San Diego, CA). Differences with *p* values of less than 0.05 were considered statistically significant.

## SUPPORTING INFORMATION

Experimental Section

Table 1. Statistics of crystallographic data and refinement

Figure S1. Typical 1D <sup>1</sup>H-NMR and 1D <sup>13</sup>C-NMR spectra

Figure S2. Screening of the adipogenic effect of hydroxamic acid-based molecules

Figure S3. Effect of **7j** on PPAR $\gamma$  transactivation and cell toxicity

Figure S4. PPAR $\delta$  transactivation activities

Figure S5. Electron density map

Figure S6. Superimposition of the crystal structures PPAR $\gamma$  / **7j** and PPAR $\gamma$  / SR2067

Figure S7. Interaction PPAR $\gamma$  /agonists

Figure S8. Adipogenic effect of the compounds

Figure S9. Effect of **7j** and Rosi on hMADS

### PDB ID

PDB 6Qj5

Authors will release the atomic coordinates and experimental data upon article publication.

## AUTHOR INFORMATION

### Corresponding Author

\* E-mail: [franck.peiretti@univ-amu.fr](mailto:franck.peiretti@univ-amu.fr)

### Author Contributions

# G. P. and J.M. B. contributed equally.

†F. P. and R. M contributed equally.

### Notes

The authors declare no competing financial interest

## ACKNOWLEDGEMENTS

This work was supported by funds from Aix Marseille University, Inserm, CNRS and ANR.

#### **ABBREVIATIONS USED**

benzotriazol-1-ylxytris(dimethylamino)phosphonium hexafluorophosphate (BOP)

human Multipotent Adipose-Derived Stem (hMADS)

non-alcoholic fatty liver disease (NAFLD)

PPAR Responsive Element (PPRE)

Rosiglitazone (Rosi)

selective PPAR $\gamma$  modulators (SPPAR $\gamma$ Ms)

Genes are identified by the symbols approved by the Human Genome Organization

## REFERENCES

- (1) Braissant, O.; Fougère, F.; Scotto, C.; Dauça, M.; Wahli, W. Differential Expression of Peroxisome Proliferator-Activated Receptors (PPARs): Tissue Distribution of PPAR-Alpha, -Beta, and -Gamma in the Adult Rat. *Endocrinology* **1996**, *137* (1), 354–366.
- (2) Botta, M.; Audano, M.; Sahebkar, A.; Sirtori, C. R.; Mitro, N.; Ruscica, M. PPAR Agonists and Metabolic Syndrome: An Established Role? *Int. J. Mol. Sci.* **2018**, *19* (4).
- (3) Derosa, G.; Sahebkar, A.; Maffioli, P. The Role of Various Peroxisome Proliferator-Activated Receptors and Their Ligands in Clinical Practice. *J. Cell. Physiol.* **2018**, *233* (1), 153–161.
- (4) Silva, A. K. S.; Peixoto, C. A. Role of Peroxisome Proliferator-Activated Receptors in Non-Alcoholic Fatty Liver Disease Inflammation. *Cell. Mol. Life Sci. CMLS* **2018**, *75* (16), 2951–2961.
- (5) Pawlak, M.; Lefebvre, P.; Staels, B. Molecular Mechanism of PPAR $\alpha$  Action and Its Impact on Lipid Metabolism, Inflammation and Fibrosis in Non-Alcoholic Fatty Liver Disease. *J. Hepatol.* **2015**, *62* (3), 720–733.
- (6) Tsunoda, F.; Asztalos, I. B.; Horvath, K. V.; Steiner, G.; Schaefer, E. J.; Asztalos, B. F. Fenofibrate, HDL, and Cardiovascular Disease in Type-2 Diabetes: The DAIS Trial. *Atherosclerosis* **2016**, *247*, 35–39.
- (7) Yaghoubi, M.; Jafari, S.; Sajedi, B.; Gohari, S.; Akbarieh, S.; Heydari, A. H.; Jameshoorani, M. Comparison of Fenofibrate and Pioglitazone Effects on Patients with Nonalcoholic Fatty Liver Disease. *Eur. J. Gastroenterol. Hepatol.* **2017**, *29* (12), 1385–1388.
- (8) Davidson, M. H.; Armani, A.; McKenney, J. M.; Jacobson, T. A. Safety Considerations with Fibrate Therapy. *Am. J. Cardiol.* **2007**, *99* (6A), 3C-18C.
- (9) Ida, S.; Kaneko, R.; Murata, K. Efficacy and Safety of Pemafibrate Administration in Patients with Dyslipidemia: A Systematic Review and Meta-Analysis. *Cardiovasc. Diabetol.* **2019**, *18* (1), 38.
- (10) Liu, Y.; Colby, J. K.; Zuo, X.; Jaoude, J.; Wei, D.; Shureiqi, I. The Role of PPAR- $\delta$  in Metabolism, Inflammation, and Cancer: Many Characters of a Critical Transcription Factor. *Int. J. Mol. Sci.* **2018**, *19* (11).
- (11) Wu, C.-C.; Baiga, T. J.; Downes, M.; La Clair, J. J.; Atkins, A. R.; Richard, S. B.; Fan, W.; Stockley-Noel, T. A.; Bowman, M. E.; Noel, J. P.; et al. Structural Basis for Specific Ligation of the Peroxisome Proliferator-Activated Receptor  $\delta$ . *Proc. Natl. Acad. Sci. U. S. A.* **2017**, *114* (13), E2563–E2570.
- (12) Olefsky, J. M. Treatment of Insulin Resistance with Peroxisome Proliferator-Activated Receptor Gamma Agonists. *J. Clin. Invest.* **2000**, *106* (4), 467–472.
- (13) Abbas, A.; Blandon, J.; Rude, J.; Elfar, A.; Mukherjee, D. PPAR-  $\gamma$  Agonist in Treatment of Diabetes: Cardiovascular Safety Considerations. *Cardiovasc. Hematol. Agents Med. Chem.* **2012**, *10* (2), 124–134.
- (14) Kung, J.; Henry, R. R. Thiazolidinedione Safety. *Expert Opin. Drug Saf.* **2012**, *11* (4), 565–579.
- (15) Balint, B. L.; Nagy, L. Selective Modulators of PPAR Activity as New Therapeutic Tools in Metabolic Diseases. *Endocr. Metab. Immune Disord. Drug Targets* **2006**, *6* (1), 33–43.
- (16) Higgins, L. S.; Depaoli, A. M. Selective Peroxisome Proliferator-Activated Receptor Gamma (PPAR $\gamma$ ) Modulation as a Strategy for Safer Therapeutic PPAR $\gamma$  Activation. *Am. J. Clin. Nutr.* **2010**, *91* (1), 267S-272S.
- (17) Choi, J. H.; Banks, A. S.; Estall, J. L.; Kajimura, S.; Boström, P.; Laznik, D.; Ruas, J. L.; Chalmers, M. J.; Kamenecka, T. M.; Blüher, M.; et al. Anti-Diabetic Drugs Inhibit

- Obesity-Linked Phosphorylation of PPARgamma by Cdk5. *Nature* **2010**, *466* (7305), 451–456.
- (18) Choi, J. H.; Banks, A. S.; Kamenecka, T. M.; Busby, S. A.; Chalmers, M. J.; Kumar, N.; Kuruvilla, D. S.; Shin, Y.; He, Y.; Bruning, J. B.; et al. Antidiabetic Actions of a Non-Agonist PPAR $\gamma$  Ligand Blocking Cdk5-Mediated Phosphorylation. *Nature* **2011**, *477* (7365), 477–481.
- (19) Balakumar, P.; Mahadevan, N.; Sambathkumar, R. A Contemporary Overview of PPAR $\alpha/\gamma$  Dual Agonists for the Management of Diabetic Dyslipidemia. *Curr. Mol. Pharmacol.* **2019**, *12* (3), 195–201.
- (20) Fiévet, C.; Fruchart, J.-C.; Staels, B. PPARAlpha and PPARgamma Dual Agonists for the Treatment of Type 2 Diabetes and the Metabolic Syndrome. *Curr. Opin. Pharmacol.* **2006**, *6* (6), 606–614.
- (21) Jani, R. H.; Pai, V.; Jha, P.; Jariwala, G.; Mukhopadhyay, S.; Bhansali, A.; Joshi, S. A Multicenter, Prospective, Randomized, Double-Blind Study to Evaluate the Safety and Efficacy of Saroglitazar 2 and 4 Mg Compared with Placebo in Type 2 Diabetes Mellitus Patients Having Hypertriglyceridemia Not Controlled with Atorvastatin Therapy (PRESS VI). *Diabetes Technol. Ther.* **2014**, *16* (2), 63–71.
- (22) Pai, V.; Paneerselvam, A.; Mukhopadhyay, S.; Bhansali, A.; Kamath, D.; Shankar, V.; Gambhire, D.; Jani, R. H.; Joshi, S.; Patel, P. A Multicenter, Prospective, Randomized, Double-Blind Study to Evaluate the Safety and Efficacy of Saroglitazar 2 and 4 Mg Compared to Pioglitazone 45 Mg in Diabetic Dyslipidemia (PRESS V). *J. Diabetes Sci. Technol.* **2014**, *8* (1), 132–141.
- (23) Giampietro, L.; Laghezza, A.; Cerchia, C.; Florio, R.; Recinella, L.; Capone, F.; Ammazalorso, A.; Bruno, I.; De Filippis, B.; Fantacuzzi, M.; et al. Novel Phenyldiazanyl Fibrate Analogues as PPAR  $\alpha/\gamma/\delta$  Pan-Agonists for the Amelioration of Metabolic Syndrome. *ACS Med. Chem. Lett.* **2019**, *10* (4), 545–551.
- (24) Laghezza, A.; Piemontese, L.; Cerchia, C.; Montanari, R.; Capelli, D.; Giudici, M.; Crestani, M.; Tortorella, P.; Peiretti, F.; Pochetti, G.; et al. Identification of the First PPAR $\alpha/\gamma$  Dual Agonist Able To Bind to Canonical and Alternative Sites of PPAR $\gamma$  and To Inhibit Its Cdk5-Mediated Phosphorylation. *J. Med. Chem.* **2018**, *61* (18), 8282–8298.
- (25) Xu, H.-R.; Zhang, J.-W.; Chen, W.-L.; Ning, Z.-Q.; Li, X.-N. Pharmacokinetics, Safety and Tolerability of Chiglitazar, A Novel Peroxisome Proliferator-Activated Receptor (PPAR) Pan-Agonist, in Healthy Chinese Volunteers: A Phase I Study. *Clin. Drug Investig.* **2019**, *39* (6), 553–563.
- (26) Gim, H. J.; Choi, Y.-S.; Li, H.; Kim, Y.-J.; Ryu, J.-H.; Jeon, R. Identification of a Novel PPAR- $\gamma$  Agonist through a Scaffold Tuning Approach. *Int. J. Mol. Sci.* **2018**, *19* (10).
- (27) Feldman, P. L.; Lambert, M. H.; Henke, B. R. PPAR Modulators and PPAR Pan Agonists for Metabolic Diseases: The next Generation of Drugs Targeting Peroxisome Proliferator-Activated Receptors? *Curr. Top. Med. Chem.* **2008**, *8* (9), 728–749.
- (28) van Marrewijk, L. M.; Polyak, S. W.; Hijnen, M.; Kuruvilla, D.; Chang, M. R.; Shin, Y.; Kamenecka, T. M.; Griffin, P. R.; Bruning, J. B. SR2067 Reveals a Unique Kinetic and Structural Signature for PPAR $\gamma$  Partial Agonism. *ACS Chem. Biol.* **2016**, *11* (1), 273–283.
- (29) Guasch, L.; Sala, E.; Valls, C.; Blay, M.; Mulero, M.; Arola, L.; Pujadas, G.; Garcia-Vallvé, S. Structural Insights for the Design of New PPARgamma Partial Agonists with High Binding Affinity and Low Transactivation Activity. *J. Comput. Aided Mol. Des.* **2011**, *25* (8), 717–728.
- (30) Eliasson, B.; Smith, U.; Mullen, S.; Cushman, S. W.; Sherman, A. S.; Yang, J. Amelioration of Insulin Resistance by Rosiglitazone Is Associated with Increased Adipose Cell Size in Obese Type 2 Diabetic Patients. *Adipocyte* **2014**, *3* (4), 314–321.

- (31) Mukherjee, R.; Hoener, P. A.; Jow, L.; Bilakovics, J.; Klausing, K.; Mais, D. E.; Faulkner, A.; Croston, G. E.; Paterniti, J. R. A Selective Peroxisome Proliferator-Activated Receptor-Gamma (PPAR $\gamma$ ) Modulator Blocks Adipocyte Differentiation but Stimulates Glucose Uptake in 3T3-L1 Adipocytes. *Mol. Endocrinol. Baltim. Md* **2000**, *14* (9), 1425–1433.
- (32) Wu, J.; Cohen, P.; Spiegelman, B. M. Adaptive Thermogenesis in Adipocytes: Is Beige the New Brown? *Genes Dev.* **2013**, *27* (3), 234–250.
- (33) Ohno, H.; Shinoda, K.; Spiegelman, B. M.; Kajimura, S. PPAR $\gamma$  Agonists Induce a White-to-Brown Fat Conversion through Stabilization of PRDM16 Protein. *Cell Metab.* **2012**, *15* (3), 395–404.
- (34) Vernochet, C.; Peres, S. B.; Davis, K. E.; McDonald, M. E.; Qiang, L.; Wang, H.; Scherer, P. E.; Farmer, S. R. C/EBP $\alpha$  and the Corepressors CtBP1 and CtBP2 Regulate Repression of Select Visceral White Adipose Genes during Induction of the Brown Phenotype in White Adipocytes by Peroxisome Proliferator-Activated Receptor Gamma Agonists. *Mol. Cell. Biol.* **2009**, *29* (17), 4714–4728.
- (35) Wu, J.; Boström, P.; Sparks, L. M.; Ye, L.; Choi, J. H.; Giang, A.-H.; Khandekar, M.; Nuutila, P.; Schaart, G.; Huang, K.; et al. Beige Adipocytes Are a Distinct Type of Thermogenic Fat Cell in Mouse and Human. *Cell* **2012**, *150* (2), 366–376.
- (36) Lin, J.; Handschin, C.; Spiegelman, B. M. Metabolic Control through the PGC-1 Family of Transcription Coactivators. *Cell Metab.* **2005**, *1* (6), 361–370.
- (37) Pisani, D. F.; Djedaini, M.; Beranger, G. E.; Elabd, C.; Scheideler, M.; Ailhaud, G.; Amri, E.-Z. Differentiation of Human Adipose-Derived Stem Cells into “Brite” (Brown-in-White) Adipocytes. *Front. Endocrinol.* **2011**, *2*, 87.
- (38) Elabd, C.; Chiellini, C.; Carmona, M.; Galitzky, J.; Cochet, O.; Petersen, R.; Pénicaud, L.; Kristiansen, K.; Bouloumié, A.; Casteilla, L.; et al. Human Multipotent Adipose-Derived Stem Cells Differentiate into Functional Brown Adipocytes. *Stem Cells Dayt. Ohio* **2009**, *27* (11), 2753–2760.
- (39) Vidal, N.; Cavaillé, J. P.; Poggi, M.; Peiretti, F.; Stocker, P. A Nonradioisotope Chemiluminescent Assay for Evaluation of 2-Deoxyglucose Uptake in 3T3-L1 Adipocytes. Effect of Various Carbonyls Species on Insulin Action. *Biochimie* **2012**, *94* (12), 2569–2576.
- (40) Pochetti, G.; Godio, C.; Mitro, N.; Caruso, D.; Galmozzi, A.; Scurati, S.; Loiodice, F.; Fracchiolla, G.; Tortorella, P.; Laghezza, A.; et al. Insights into the Mechanism of Partial Agonism: Crystal Structures of the Peroxisome Proliferator-Activated Receptor Gamma Ligand-Binding Domain in the Complex with Two Enantiomeric Ligands. *J. Biol. Chem.* **2007**, *282* (23), 17314–17324.
- (41) Kabsch, W. XDS. *Acta Crystallogr. D Biol. Crystallogr.* **2010**, *66* (Pt 2), 125–132.
- (42) Navaza, J. AMoRe: An Automated Package for Molecular Replacement. *Acta Crystallogr. A* **1994**, *50* (2), 157–163.
- (43) Brünger, A. T.; Adams, P. D.; Clore, G. M.; DeLano, W. L.; Gros, P.; Grosse-Kunstleve, R. W.; Jiang, J. S.; Kuszewski, J.; Nilges, M.; Pannu, N. S.; et al. Crystallography & NMR System: A New Software Suite for Macromolecular Structure Determination. *Acta Crystallogr. D Biol. Crystallogr.* **1998**, *54* (Pt 5), 905–921.
- (44) Adams, P. D.; Afonine, P. V.; Bunkóczi, G.; Chen, V. B.; Davis, I. W.; Echols, N.; Headd, J. J.; Hung, L.-W.; Kapral, G. J.; Grosse-Kunstleve, R. W.; et al. PHENIX: A Comprehensive Python-Based System for Macromolecular Structure Solution. *Acta Crystallogr. D Biol. Crystallogr.* **2010**, *66* (Pt 2), 213–221.
- (45) Jonsson, U.; Malmqvist, M. Real Time Biospecific Interaction Analysis. The Integration of Surface Plasmon Resonance Detection, General Biospecific Interface Chemistry and

- Microfluides into One Analytical System. In *Advances in biosensor*; 1992; Vol. 2, pp 291–336.
- (46) Quinn, J. G. Modeling Taylor Dispersion Injections: Determination of Kinetic/Affinity Interaction Constants and Diffusion Coefficients in Label-Free Biosensing. *Anal. Biochem.* **2012**, *421* (2), 391–400.

Table of Contents graphic

